MARMARA UNIVERSITY
FACULTY OF ENGINEERING

PREDICTION OF STRAIN INHOMOGENEITY AND LOAD DURING PLANAR TWIST CHANNEL ANGULAR EXTRUSION PROCESS BY ARTIFICIAL NEURAL NETWORK

Ramazan Yiğit Kaymaz 150418040

Nurullah Tekinbaş 150418054

Muhammet Efekan Yiğit 150418063

GRADUATION PROJECT REPORT

Department of Mechanical Engineering

Supervisor

Prof.Dr. AYKUT KENTLİ

ISTANBUL, 2024

MARMARA UNIVERSITY
FACULTY OF ENGINEERING

PREDICTION OF STRAIN INHOMOGENEITY AND LOAD DURING PLANAR TWIST CHANNEL ANGULAR EXTRUSION PROCESS BY ARTIFICIAL NEURAL NETWORK

By

Ramazan Yiğit Kaymaz, Nurullah Tekinbaş , Muhammet Efekan Yiğit

January 2024, Istanbul

SUBMITTED TO THE DEPARTMENT OF MECHANICAL ENGINEERING IN PARTIAL FULFILLMENT OF THE REQUIREMENTS FOR THE DEGREE

OF

BACHELOR OF SCIENCE

AT

MARMARA UNIVERSITY

Signature of Author(s)

Ramazan Yiğit Kaymaz

Nurullah Tekinbaş

Muhammet Efekan Yiğit

Department of Mechanical Engineering

Certified By ..... Prof.Dr. AYKUT KENTLİ

Project Supervisor, Department of Mechanical Engineering

Accepted By.....Prof.Dr.Bülent EKİCİ

Head of the Department of Mechanical Engineering

ACKNOWLEDGEMENT

First of all, we express our profound gratitude to our advisor, Prof.Dr. Aykut KENTLİ for his essential expertise and crucial comments provided at different phases of our project.

We express appreciation to Res.Assist.Dr. Serkan ÖĞÜT for providing us with his useful insights throughout the process of writing this thesis and doing the study, and for consistently offering his constant support.

January, 2024

Ramazan Yiğit KAYMAZ

Nurullah TEKİNBAŞ

Muhammet Efekan YİĞİT

Table of Contents

ÖZET

Malzemelerin mikroyapılarında değişiklikler yapılarak mukavemetinin arttırılması için çeşitli teknikler denenmiştir. Aşırı plastik deformasyon (APD) teknikleri, malzemenin mikro yapısında daha küçük tanecikler oluşturarak ve bu taneciklerin homojen dağılımını sağlayarak malzemenin mukavemetini arttırır. Bu çalışmada Aşırı plastik deformasyonun (APD) bir türü olan düzlemsel bükümlü kanal açısal ekstrüzyon (DBKAE) yöntemi incelenmiştir. DBKAE yönteminin amacına özel olarak bir kalıp oluşturuldu. Kalıp üzerindeki iki farklı parametre ve Deform 3D yazılımında yapılan analizler esnasında da bir parametre değiştirilerek toplam 27 sonlu eleman analizi gerçekleştirildi. Analizler sonucunda maksimum yük ve ortalama gerinim değerleri elde edildi. Elde edilen verilere dayanarak gerinim homojensizliğinin değeri de hesaplandı. Elde edilen bu değerlere doğrultusunda MATLAB yazılımı kullanılarak bir yapay zeka ağı (YSA) geliştirildi. Bu yapay zeka ağı, minimum hata payıyla yük değerleri ile elde edilen veriler arasındaki ilişkiyi modellemektedir.

ABSTRACT

Several techniques have been used to improve the mechanical strength of materials through modifications in their microstructural structure. Severe plastic deformation (SPD) procedures enhance the material's strength by generating smaller grains within its microstructure and ensuring a uniform distribution of these grains. This study investigated the planar twisted channel angular extrusion (PTCAE) method, which is a sort of severe plastic deformation (SPD). A die was specifically designed for the implementation of the PTCAE technique. In the Deform 3D programme, a series of 27 finite element analyses were conducted by modifying two distinct parameters on the die and one parameter throughout the study. The analyses yielded maximum load and average strain values. The value of strain inhomogeneity was computed based on the acquired data. Based on these acquired values, a MATLAB software was utilised to create an artificial neural network (ANN). This artificial neural network accurately simulates the relationship between load levels and the acquired data with minimal margin of error.

SYMBOLS

Φ: Abrupt Angle

Ψ: Arc of Curvature

α: Planar Twist Angle (Alpha Angle)

mm: Millimeter

°C: Degree Celsius

N: Newton

°: Degree Angle

n : Safety Factor

σ_y : Yield Strength

σ : Stress

F : Force

A : Area

E : Young's Modulus

I : Moment of Inertia

L = Length

p_{CR} : Critical Load

ABBREVIATIONS

NSM: Nanostructured Materials

SPD: Severe Plastic Deformation

ECAP: Equal Channel Angular Pressing

HPT: High Pressure Torsion

TE: Twisted Extrusion

VF: Versatile Forging

RCS: Repeated Corrugation and Straightening

CGP: Constrained Groove Pressing

CCC: Cylinder Covered Compression

ARB: Accumulative Roll Bonding

FSP: Friction Stir Processing

SFSP: Submerged Friction Stir Processing

IECAP: Incremental Equal-Channel Pressing

TMCAP: Multi-Channel Angular Pressing

TWO-CAP: Thin-Walled Open-Channel Angular Pressing

EXP-ECAP: Expansion Equal Channel Angular Pressing

PTCAE: Planar Twist Channel Angular Extrusion

ANN: Artificial Neural Network

FE: Finite Element

LIST OF FIGURES

LIST OF TABLES

1.INTRODUCTION

In recent years, there has been an increasing interest among materials science professionals in bulk nanostructured materials (NSM) that are manufactured using severe plastic deformation (SPD) techniques [1]. SPD procedures refer to material forming techniques that subject a bulk material to a significant amount of plastic deformation, resulting in the formation of ultra-fine grained (UFG) material [2]. SPD technologies are becoming more popular due to their capacity to reduce the grain size of materials to the sub-micrometer or nanoscale scale. The refinement of grains relates to the formation of various flaws in the lattice, which leads to variance in the produced microstructure [3]. Consequently, these characteristics lead to enhanced mechanical and functional properties, including exceptional strength, a reduced elasticity coefficient, remarkable toughness, heightened diffusion activation, and superior super plasticity at low temperatures. When comparing to their coarse-grained counterparts, these qualities are often superior in materials that have undergone SPD processing [4]. When creating methods for severe plastic deformation to generate nanostructures in bulk samples and billets, it is important to consider a set of criteria. The following are the specified prerequisites. Firstly, it is essential to achieve ultra-fine-grained structures with predominant high-angle grain boundaries. This is because only under these conditions can a significant change in material characteristics take place. Furthermore, achieving homogeneous nanostructure creation across the whole volume of a sample is essential in order to ensure the stability of the treated materials' attributes. Furthermore, it is essential that samples do not exhibit any mechanical damage or fractures, while being subjected to significant plastic deformations. Conventional techniques for extreme plastic deformation, such as rolling, drawing, or extrusion, are inadequate to fulfil these criteria. The production of nanostructures in bulk samples requires the use of certain mechanical deformation techniques that allow for significant deformations at relatively low temperatures. Additionally, it is necessary to determine the appropriate processing conditions for the material [5]. Currently, there are many SPD techniques accessible for creating metals with very fine grain sizes. These techniques are, Equal Channel Angular Pressing(ECAP) [6], where it is also studied by Patrick B. Berbon, Minoru Furukawa, Zenji Horita, Minoru Nemoto, And Terence G. Langdon. In their study, an investigation was conducted to examine the impact of pressing speed on equal-channel angular (ECA) pressing, utilizing samples of pure aluminum. High Pressure Torsion (HPT) [7], where it is studied by A.P. Zhilyaev, G.V. Nurislamovac, B-K. Kim, M.D. Baro, J.A. Szpunar, T.G. Langdon. Their objective is to examine the experimental factors that affect the refining of grains and the development of microstructure during the HPT process using pure nickel. Twisted Extrusion (TE) [8], where it is studied by H. Zendehdel, A. Hassani, aiming to investigate mechanical properties of aluminum alloy 6063 before and after TE process. Repeated Corrugation and Straightening (RCS) [9], where it is studied by H. Abolfathi, H.R. Jafarian, H. Arabi, N. Park, A.R. Eivani, studying the impact of recurrent corrugation and straightening by rolling (RCSR) procedure on the microstructural development and tensile characteristics of a Fe-24Ni-0.3C Transformation Induced Plasticity (TRIP) steel. Multi-Directional Forging (MDF) [10], where it is studied by C. Kobayashi, T. Sakai, A. Belyakov, And H. Miura. Their study focused on investigating the development of ultrafine grains in pure copper by the process of multidirectional forging (MDF) at a temperature of 195K. Cyclic-Extrusion-Compression [11], where it is studied by Jinbao Lin, Qudong Wang, Liming

Peng, Hans J. Roven. Their study is aimed to study the plastic deformation characteristics and strain homogeneity of the ZK60 magnesium alloy during the multi-pass cyclic extrusion and compression (CEC) process. Reciprocating Extrusion [12], Constrained Groove Pressing (CGP) [13], Cylinder Covered Compression (CCC) [14], Accumulative Roll Bonding (ARB) [15], Friction Stir Processing (FSP) [16], and Submerged Friction Stir Processing (SFSP) [17]. Among these many techniques, equal-channel angular pressing stands out as a particularly appealing processing approach for numerous reasons. Firstly, this technique may be employed on rather large billets, allowing to produce materials that have the potential to be used in a diverse array of structural applications. Furthermore, the technique of Equal Channel Angular Pressing (ECAP) is uncomplicated and can be effortlessly executed on many alloys. The only exception is the fabrication of the die since the equipment required for ECAP is commonly accessible in most laboratory settings. Furthermore, ECAP has the potential to be used in the processing of materials with diverse crystal structures, including a wide range of materials such as precipitation-hardened alloys, intermetallic, and metal-matrix composites. Furthermore, a desirable level of uniformity is achieved in most of the billet when the pressing process is carried out to a significant degree of deformation. Furthermore, it is possible to increase the size of the process for pressing relatively big samples. Additionally, there is a promising opportunity to use ECAP in commercial metal-processing methods. The presence of these diverse appealing characteristics has prompted several experimental investigations and novel advancements in ECAP processing within the last decade.[18] During the ECAP process, the sample is compressed as it flows through the channel, causing a shear strain to occur at the bending point of the channel. Repetitive pressing is possible since the sample cross-section stays constant. The sample undergoes a significant amount of strain, resulting in grain refinement by recurrent pressing [19]. A depiction of the ECAP process can be seen in figure 1.1.

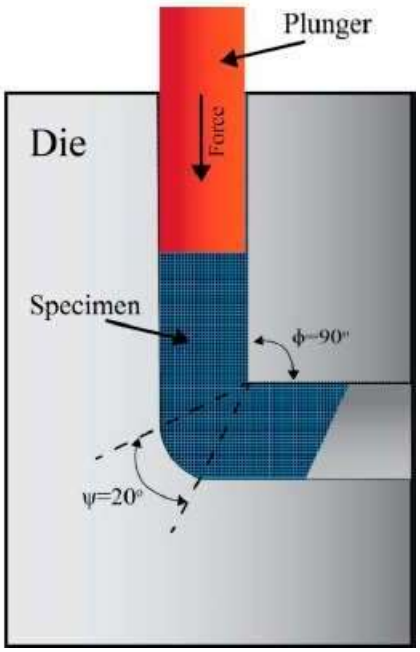

Figure 1.1: A diagram depicting the equal channel angular pressing technique. [20]

Figure 1 depicts a cross-section of the die, indicating two internal angles, Φ and Ψ, which determine the curvature of the two channels. The angle Φ represents the separation between the channels, while the angle Ψ is located at the outer arc of curvature where the two channels meet [21]. Since the design phase, the technique has been extensively modified and modernized in terms of die design, processing pathways, and the use of various experimental factors to increase the efficiency of the process and avoid limitations. For example, in ECAP process, it is necessary to withdraw the sample from the die and then to reinsert it in order to get a high imposed strain and a large number of passes, which makes it labor-intensive and time consuming.[22] As a result, many modifications of ECAP processes are presented such as Incremental Equal-Channel Pressing (IECAP)[23], Twisted Multi-Channel Angular Pressing (TMCAP)[24], Thin-Walled Open-Channel Angular Pressing (TWO-CAP) [25], Expansion Equal Channel Angular Pressing (Exp.-ECAP) [26], and Planar Twist Channel Angular Extrusion (PTCAE) [27] have been proposed. Within this study, PTCAE method, which is one of the methods mentioned above, will be studied.

The PTCAE method is derived from the classical equal channel angular pressing technique, but itinvolves the application of extra planar twist strain in the deformation zone of ECAP at the same time. The cross-sectional area of the sample stays unchanged throughout this operation. Successiverepetition of this procedure is a key prerequisite for SPD processes [28]. Schematics of PTCAE process are shown in figure 1.2.

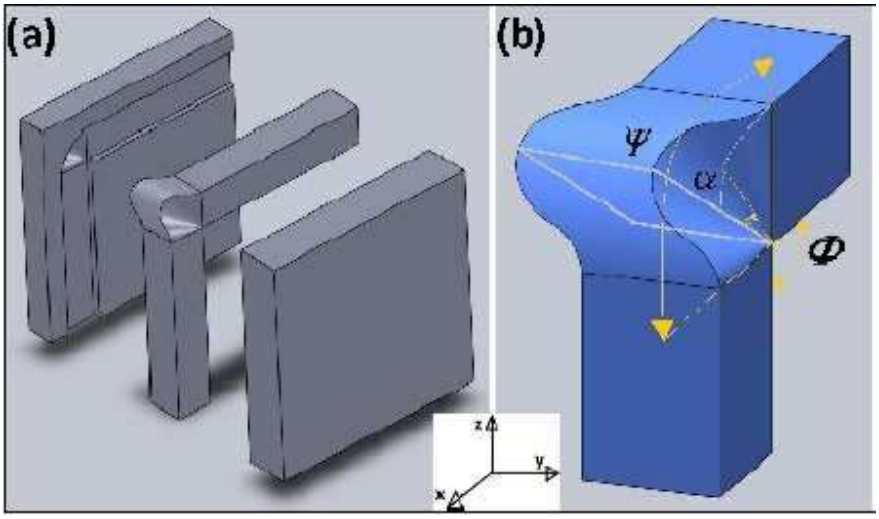

Figure 1.2: Schematic illustration of PTCAE process.[29]

Figure 2 illustrates the presence of three angles (Φ, Ψ, and α) in the PTCAE process, with Φ and Ψ being identical angles that also occur in the ECAP process. There exists an extra angle, α, which denotes the angle related to the lateral reversal arc of curvature in the deformation zone. Put simply, α starts at zero at the entry of the deformation zone, reaches its maximum value in the middle of the deformation zone path, and returns to zero at the exit of the deformation zone. The imposed deformation caused by the α angle is characterized by shear deformation, which happens as the sample goes through the die.[29] The primary benefits of this process, when compared to other SPD methods, include the simultaneous application of plastic shear strain in three perpendicular planes within a single deformation zone, a small volume of plastic deformation, fewer required passes to achieve material with the desired grain size, reduced extrusion load due to decreased contact surfaces between the sample and the die, and ultimately, improved processing efficiency.[29], [30]. When the literature is reviewed, it is seen that there is a direct relationship between the processing load, average strain, and planar twist angle (α). This study examines the processing load and inhomogeneity of effective strain in the PTCAE process for various planar twist angles (α), ram speeds, and fillets. In order to facilitate better comparisons across various processing circumstances, the other parameters involved in the process, such as the friction coefficient, meshing size and type, abrupt angle (Φ), and arc of curvature (Ψ), were kept constant. Additionally, for these variations, predicted processing average load and effective strains by Artificial Neural Network (ANN) models will be considered.

2. METHODS

2.1. FE ANALYSES

CATIA V5 software was used for the design and construction of the workpiece, die, and plunger in 3D modeling. The workpiece will be moved along the die by the plunger and will pass through the angled section. As a result, ongoing changes in load and force will be experienced by the workpiece, which will be subjected to a constant velocity. The aim is to increase the strength of the workpiece in accordance with the specified angles, plunger speeds, and radius values. The workpiece and the channel it will go through both have a length of 70 mm. Additionally, they have identical width and height, measuring 10 mm each. The following 3-D models of workpiece, plunger and die can be checked below.

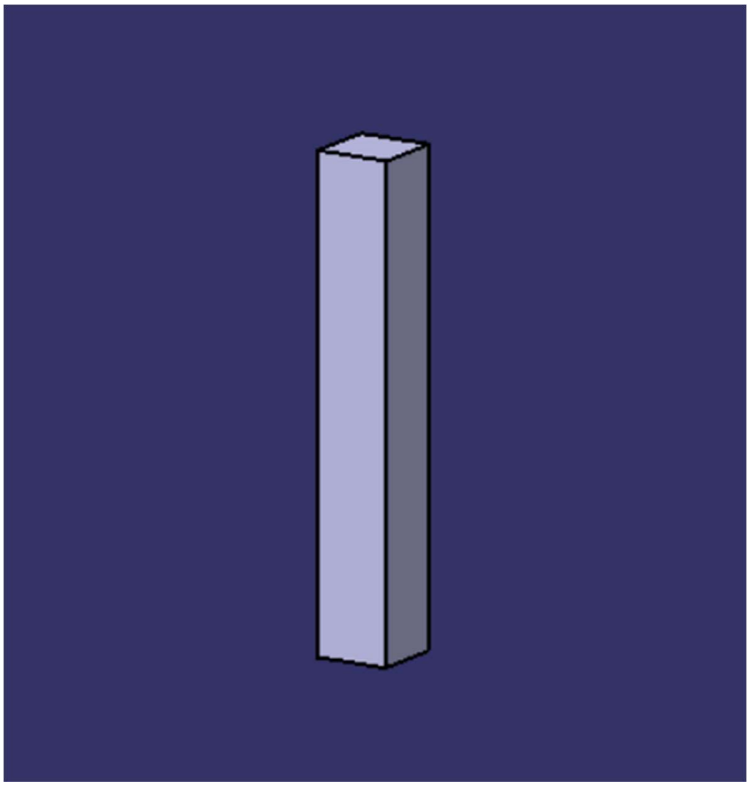

Figure 2.1: 3-D Model of the workpiece.

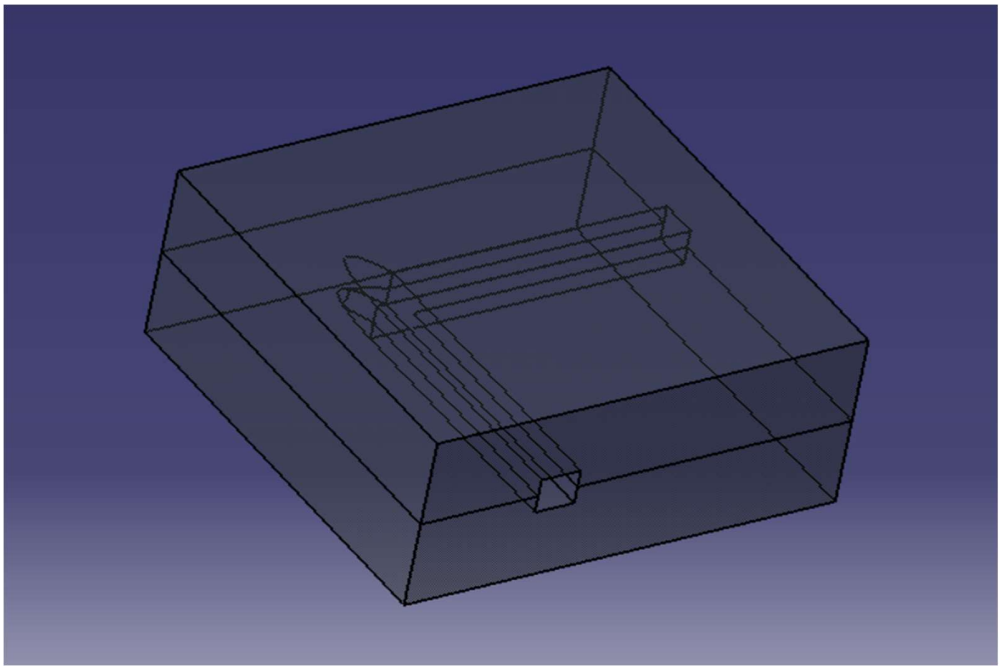

Figure 2.2: 3-D Model of the die.

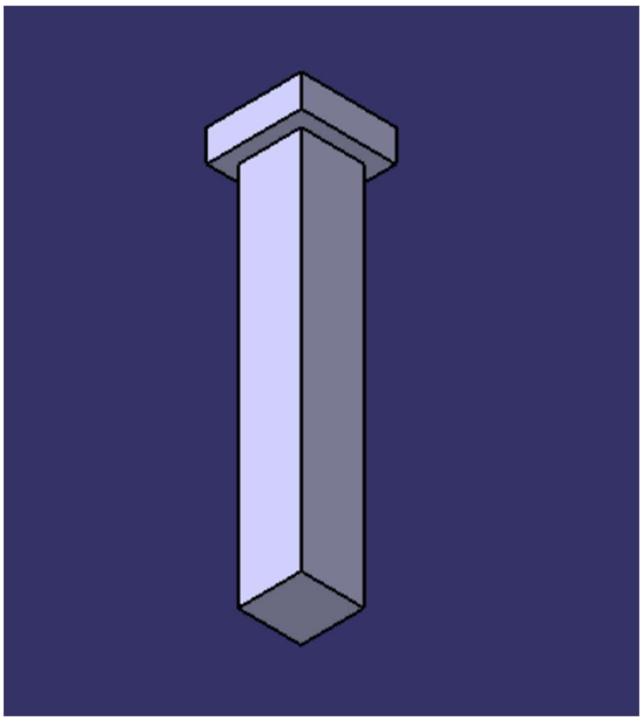

Figure 2.3: 3-D Model of the plunger.

To increase the experimental consistency, a total of 27 combinations were made. The possibilities were generated by utilizing 3 distinct alpha angles, 3 varying plunger speeds, and 3 different radius values. The friction factor was determined as 0.1 [31] . During the process of determining this value, literature review [32] is taken as an aspect of reference. The table below indicates the parameters employed for each experiment.

Table 2.1: Parameters matrix for FE analyses

Analysis No	Alpha Angle	Radius	Ram Speed
1	0,00	0,00	1,00
2	0,00	0,00	4,00
3	0,00	0,00	7,00
4	0,00	1,50	1,00
5	0,00	1,50	4,00
6	0,00	1,50	7,00
7	0,00	3,00	1,00
8	0,00	3,00	4,00
9	0,00	3,00	7,00
10	20,00	0,00	1,00
11	20,00	0,00	4,00
12	20,00	0,00	7,00
13	20,00	1,50	1,00
14	20,00	1,50	4,00
15	20,00	1,50	7,00
16	20,00	3,00	1,00
17	20,00	3,00	4,00
18	20,00	3,00	7,00
19	40,00	0,00	1,00
20	40,00	0,00	4,00
21	40,00	0,00	7,00
22	40,00	1,50	1,00
23	40,00	1,50	4,00
24	40,00	1,50	7,00
25	40,00	3,00	1,00
26	40,00	3,00	4,00
27	40,00	3,00	7,00

The parameter specified as alpha angle indicates the value of the angular area in the channel shown in the figure below. With an increase in the alpha angle, there is a corresponding rise in the degree of bending of the workpiece.

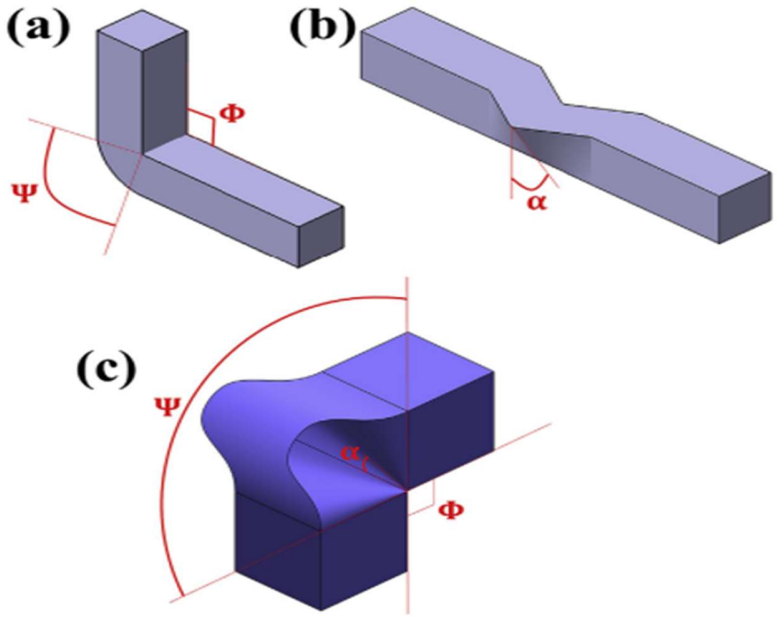

Figure 2.4: Schematic representation of a) equal channel angular pressing, b) planar twist angular channel extrusion.

The parameter identified as Radius represents the assigned radius value to facilitate a smooth transition into the 90-degree part of the channel depicted below. Thanks to this radius, the anticipation is to prevent sudden tension loads that could potentially affect the workpiece.

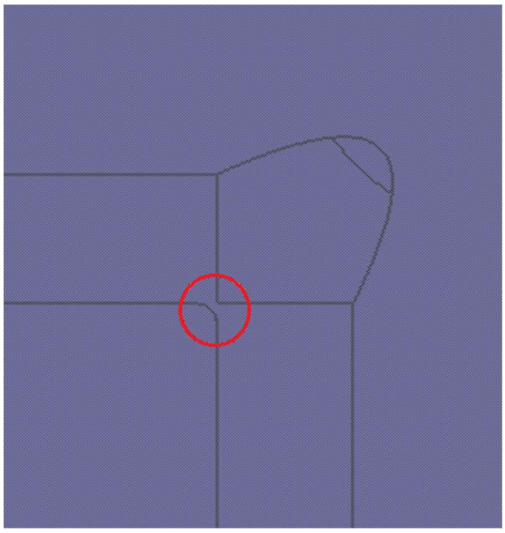

Figure 2.5: Image depicting the radius connected to the transition region of the die.

The parameter specified as ram speed indicates the speed at which the plunger pushes the workpiece in the die.

2.2. FINITE ELEMENT ANALYSIS (FEA)

All analyzes were performed using DEFORM 3D. Some unexpected results occurred in some of the experiments. Some of the results obtained at maximum loads are the workpiece being overstressed during unexpected strokes. It was also foreseen that unexpected individual errors might occur due to the interactions between these three parameters which are used. The die was kept constant throughout the analysis and no material assignment was made. The die was not exposed to any bending or deformation.

The International System of Units (SI) was used in the analysis performed with DEFORM 3D software. A cold forming technique was used. Consequently, the moderate option was selected to address both complexity and accuracy elements within the model complexity section. By minimizing the margin of error throughout the analytical process, results that accurately reflect reality were able to be provided. As part of the ongoing study, the first step involved importing the

workpiece and applying meshing using the DEFORM 3D software. The workpiece material selected was AL-1100 due to its favorable characteristics at a cold temperature of 70°F (20°C).

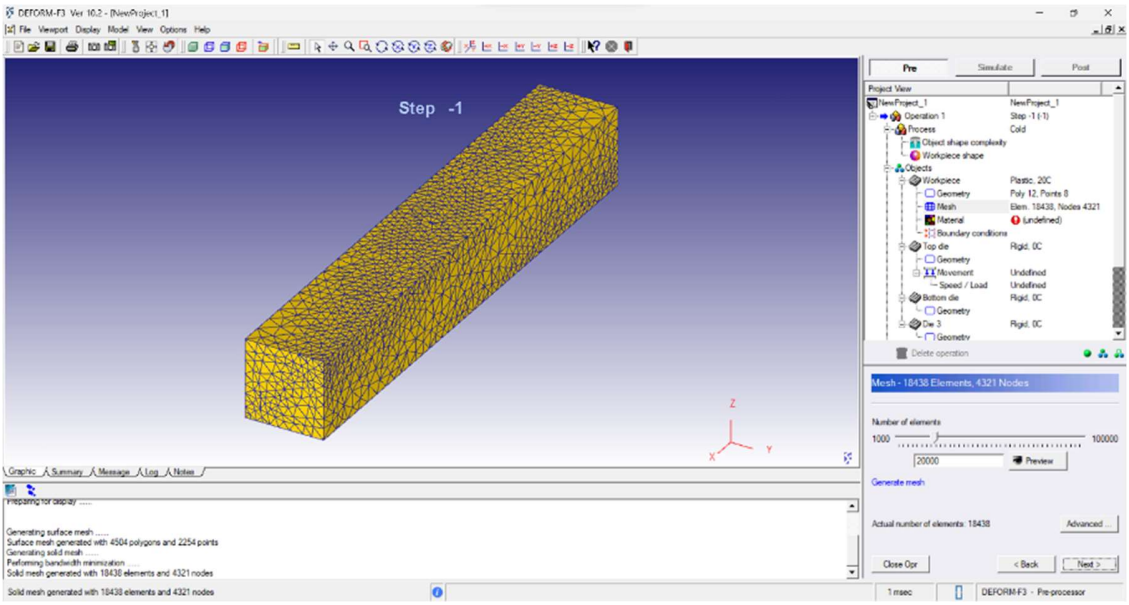

Figure 2.6: Workpiece after meshing is applied.

Following that, the plunger component was imported. The speed/load section is calibrated based on the orientation of the assembly generated by the CATIA V5 software. Three distinct speed magnitudes are assigned during the analyses. Assignment of speed magnitude and directions are provided below.

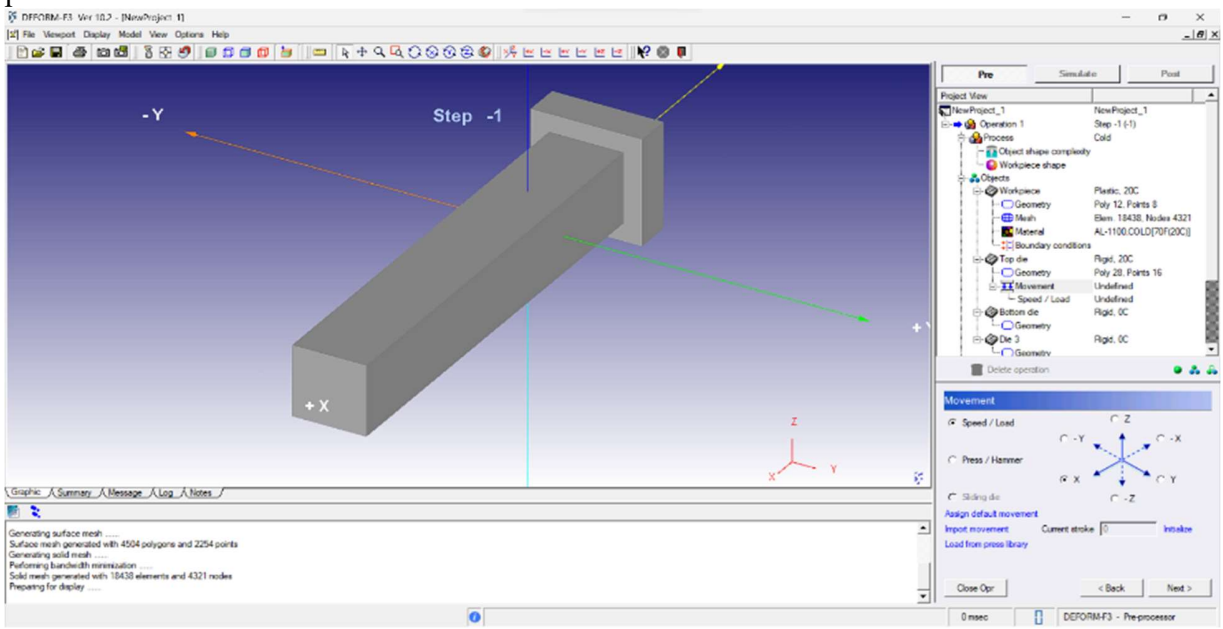

Figure 2.7: Assigning direction and magnitude of the plunger speed.

Following that, the top die, designed in CATIA V5 software, was imported and subsequently fixed within the existing geometry. Following the same method, the lower die was imported by ensuring the geometry is properly aligned. Then, friction coefficient is specified as 0.1 and contact nodes are generated. Extrusion stroke is specified as 65mm, which determines the distance that plunger should follow. In the stop control section, an option was chosen to limit the die stroke, preventing it from exceeding the specified route input. After completing the data verification process and initiating the database generation, the operational phase was completed, leading to the simulation section analysis.

Throughout the analysis process, the progressive degradation of the structure was observed using simulation display. The capability to see stroke and strain levels allowed for immediate observation of the results. The relevant images are displayed below.

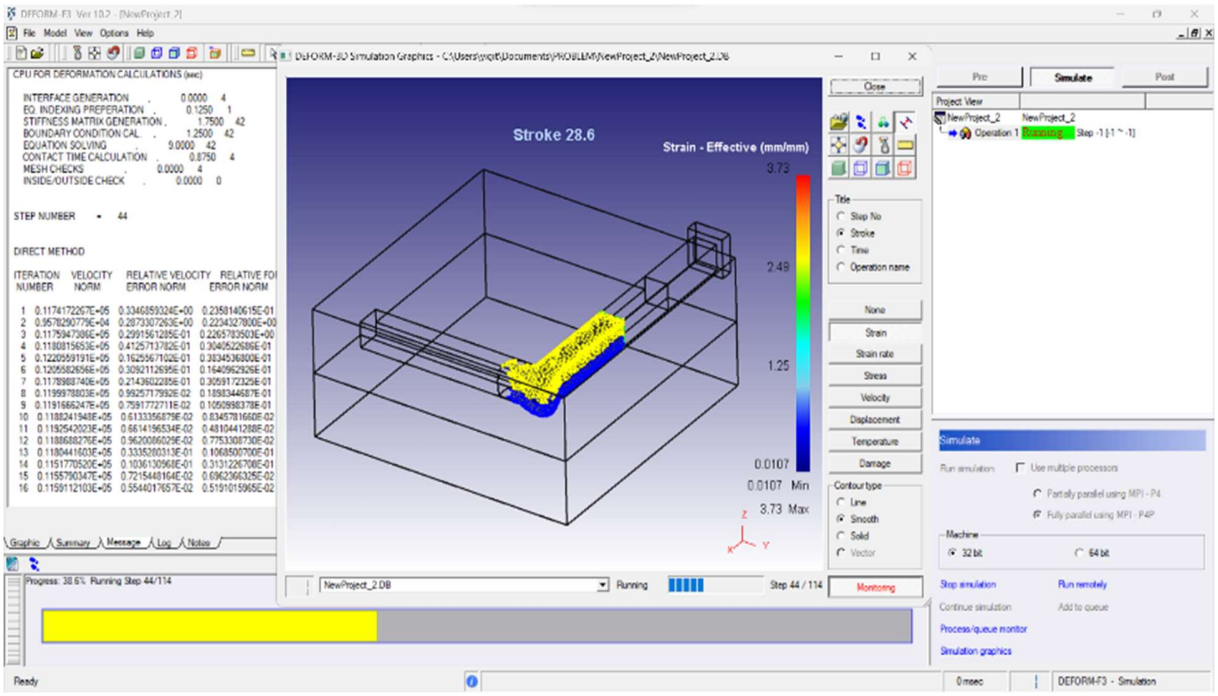

Figure 2.8: Image showing the process during simulation.

After completion of the analysis, the post-processing phase proceeded. After the analysis conclusion, a graph was generated to visually depict the stroke and load values on the workpiece. This facilitated systematic monitoring of these values to observe the analysis conducted. Within this graph, the interval when the stroke value reached its highest point was determined, and all load magnitudes at each stroke were documented in Excel spreadsheet.

Graphs illustrating the stroke values of workpiece during the study are generated. This process was executed separately for each of the 27 analyses conducted. The graphs were stored in an Excel file,

enabling the computation of average, standard deviation, maximum load values, and strain inhomogeneity index, which is the proportion of the average strain to standard deviation, for each analysis performed. The inclusion of second order smoothing in the graph creation process facilitated obtaining a smooth representation of data. This refinement aided in achieving more detailed and visually refined representations for the studies.

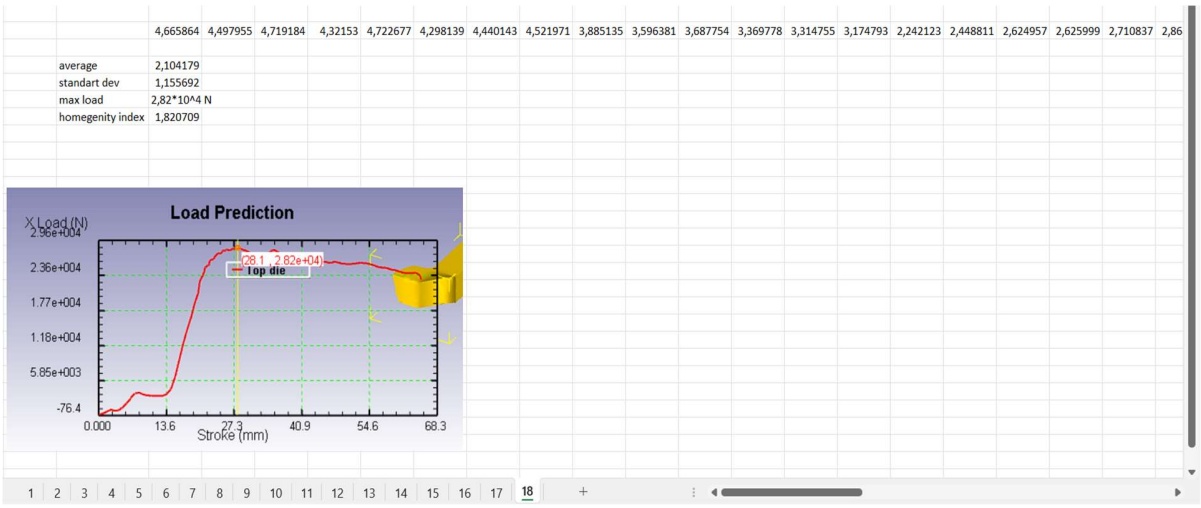

Figure 2.9: Data exporting process and example of the excel spreadsheet.

The mean load values were calculated to assess the cumulative outcomes of all analyses. These numbers were computed for each analysis performed and documented accordingly. Subsequently, the component was cut along the y-axis using the slicing command to enable effective strain evaluation. The strain scaling section was set to a maximum value of 4 in the setup. The 'solid shading' option in the plot type section was selected to adjust the degree of solidity during transitions.

After the analysis, the predetermined point data was entered into the DEFORM 3D software, ensuring precise alignment with the points on the workpiece. Utilizing point tracking, the data was captured and subsequently transferred into an Excel spreadsheet. The point tracking of strain on the material and obtaining the graph process can be checked below.

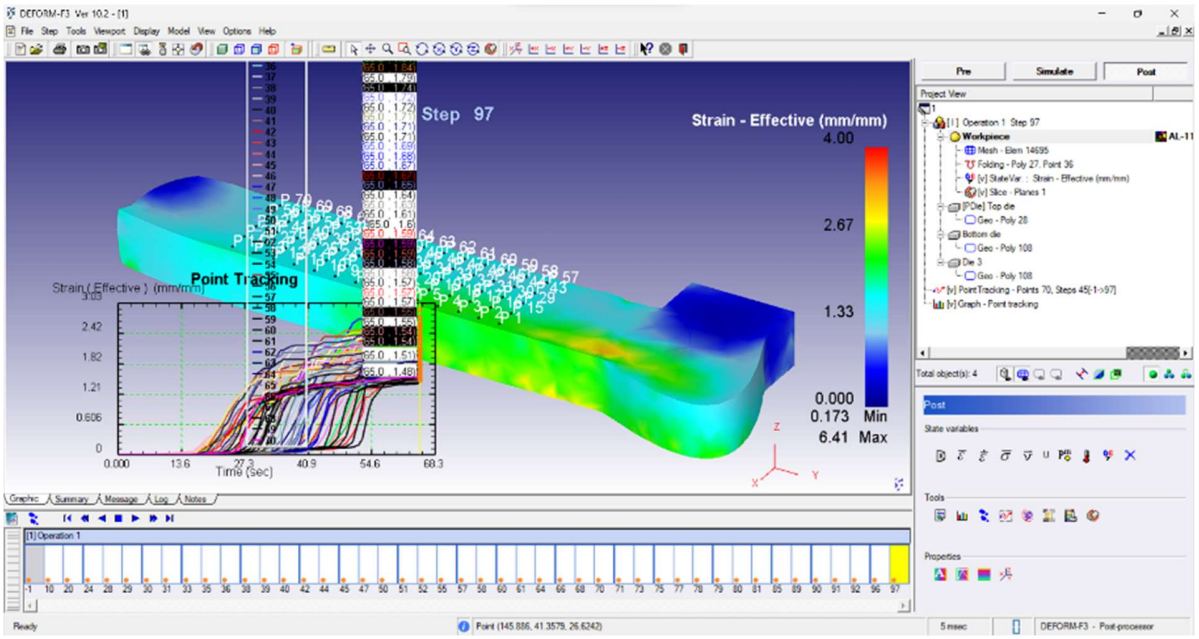

Figure 2.10: Point attachment on the workpiece and obtaining the graphs with point tracking.

2.3. ARTIFICAL NEURAL NETWORK (ANN)

The study employed ANN in place of iterative simulations across diverse domains such as engineering and materials science. ANN have demonstrated efficacy in forecasting material properties and process variables, especially in the optimization of die design for the ECAP technique, resulting in a substantial simplification of forecasts. This study utilized ANN implemented in MATLAB to create models that represent the relationship between ECAP die angle data acquired from FE analysis.

The ANN was trained using a dataset that consisted of input features and their associated target values. The objective of the training was to minimize the errors in the predictions made by the ANN. The target matrix included load values obtained from finite element analysis, while the input matrix consisted of the angle (Alpha), die radius, and ram speed. Initially, different quantities of concealed neurons were experimented with using the variable "numHiddenNeurons" and the most optimal outcome was obtained with 7 neurons. As a result, the number of hidden neurons was determined to be 7 and the network was initialized using the "newfit" command, which creates the network based on the provided inputs and targets. Subsequently, the training parameters of the network were determined to achieve a specific goal, while ensuring a target error tolerance of 10^6. The training of the ANN required the division of the dataset into two distinct subsets. The given datasets comprise of a training set and a test set. The training set encompassed 70% of the data, whereas the test set constituted 30%. The "trainlm" command was used to decrease the disparity between the anticipated outputs and the targets during the training phase. The Levenberg-Marquardt performance function was chosen to be utilized in the artificial intelligence network. In addition, the neural network model's performance was evaluated using the "mean absolute error" performance metric, which measures the difference between the model's predictions and the actual values during the training phase. To evaluate the performance of both the training and test datasets, graphical representations are generated. A regression graph was constructed using the "plotregression" command to examine the association between the target values and the outputs produced by the trained network. The collected errors were categorized as training and test errors, and they were stored in Excel by using the “xlswrite" command. This file contains the overall differences between the network's predicted values and the desired values, as well as the desired values and their corresponding actual values for both the training and test datasets. The Excel file also includes minimum, maximum, and average error numbers, which aid in conducting further examination and evaluations. Furthermore, the "plotperf" and "plotfit" commands were utilized to evaluate the effectiveness of the network and demonstrate the correlation between the inputs and targets of the ANN.

3. RESULTS

3.1. FINITE ELEMENT ANALYSIS (FEA)

3.1.1 Average Load

The processing average load and values of effective strain are analyzed and read through the Deform 3-D software. The final shape of the workpiece can be seen in figure 2.1, after it completes its path through the die.

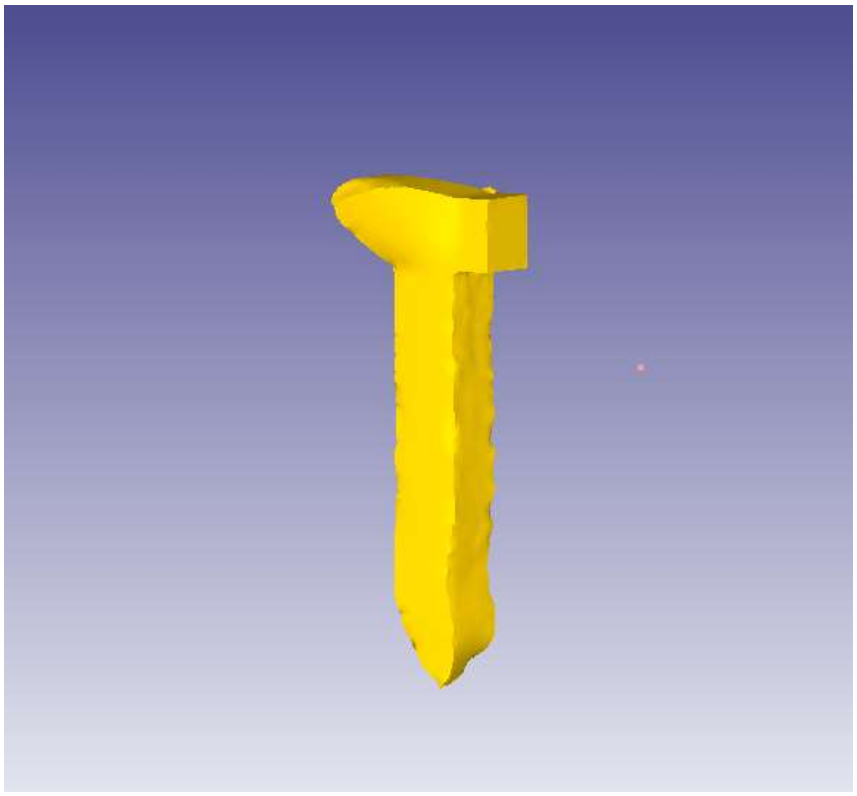

Figure 3.1: Final form of workpiece.

The average applied load during PTCAE process for each analysis numbers are given on the table 3.1 below.

Table 3.1: Average load for each analysis.

Analysis No	Max load (N)
1	19951,7484
2	21698,7116
3	20229,2426
4	18780,2465
5	19672,6239
6	19909,0035
7	19346,8236
8	19676,7108
9	18680,3858
10	22094,5475
11	21900,9149
12	21384,1049
13	20010,9192
14	19966,3919
15	19487,9393
16	20223,1469
17	23131,0175
18	20674,4212
19	23937,9350
20	23245,4770
21	23354,8296
22	23165,9228
23	22652,4396
24	23036,1759
25	21585,9624
26	21344,7973
27	22452,1475

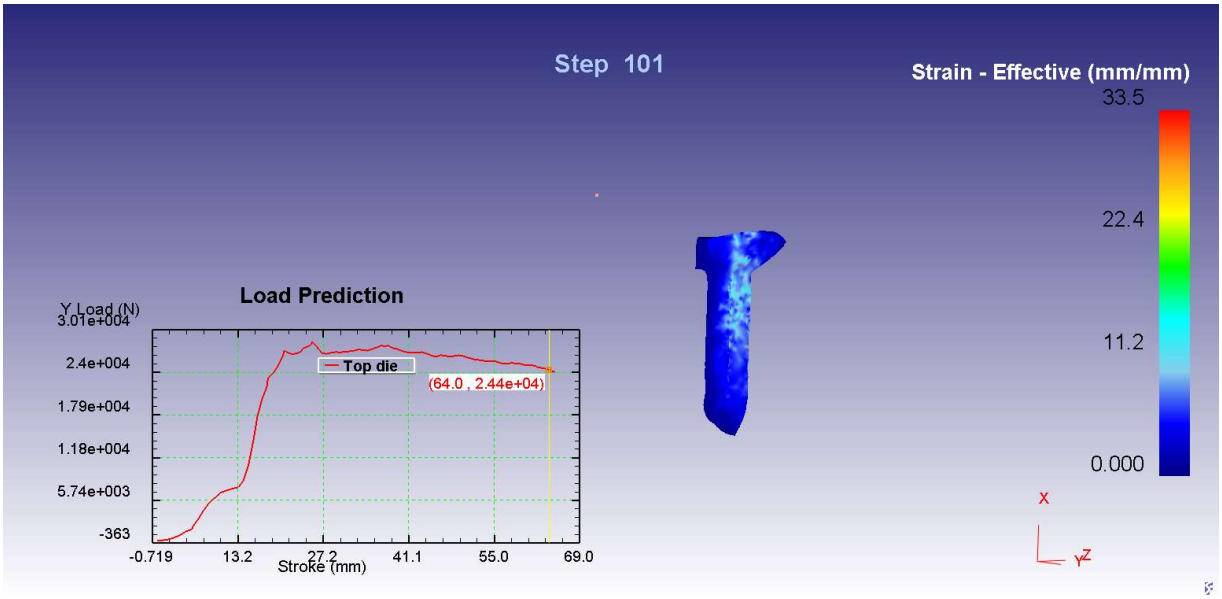

Figure 3.2: Load prediction graph of 26th analysis as an example.

When analyzing load prediction values, the 2nd order smoothing technique is used in order to avoid instantaneous fluctuations and make a clear interpretation of values.

On the other hand, the effect of angle α, fillets on the die, and ram speed can be checked on figures given below.

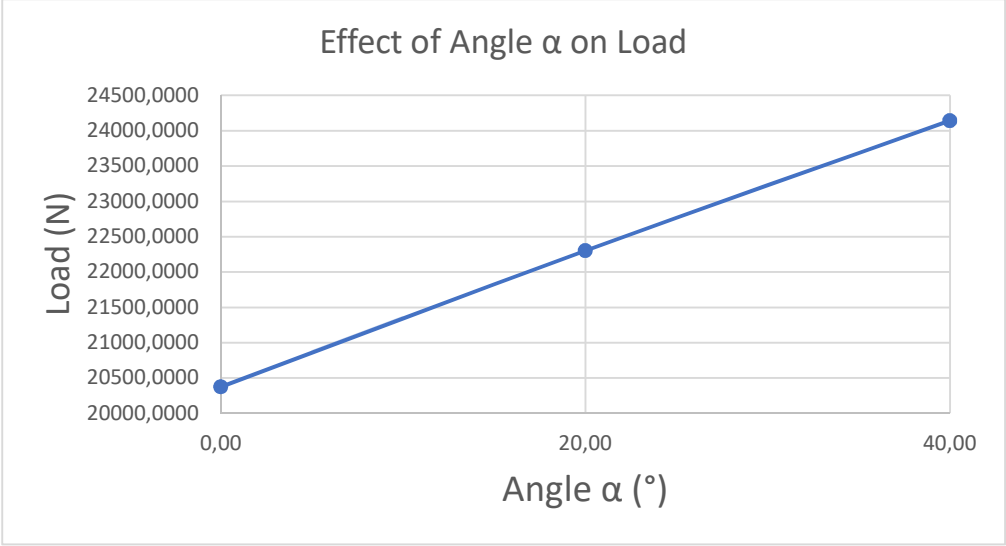

Figure 3.3: Effect of angle α on load.

On figure 3.3, results show that with the increase of angle α, there is a significant amount of increase in both average load and effective strain. As the planar twist angle rises, the length of contact between the material and plunger also increases. This increase results in elevated energy levels, thereby leading to a larger processing load. As a result, this inference matches with the reference study [29]

On figure 3.3, analysis 1, 10 and 19 are taken as an example where other parameters are kept constant.

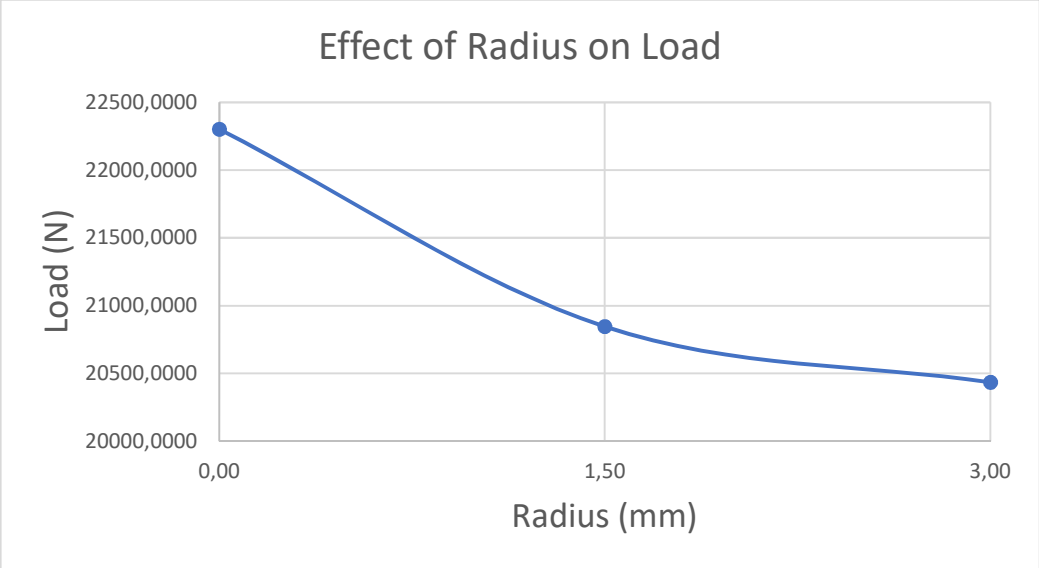

Figure 3.4: Effect of radius on load.

For this comparison on figure 3.4, results of analysis 10, 13 and 16 are exported as an example.

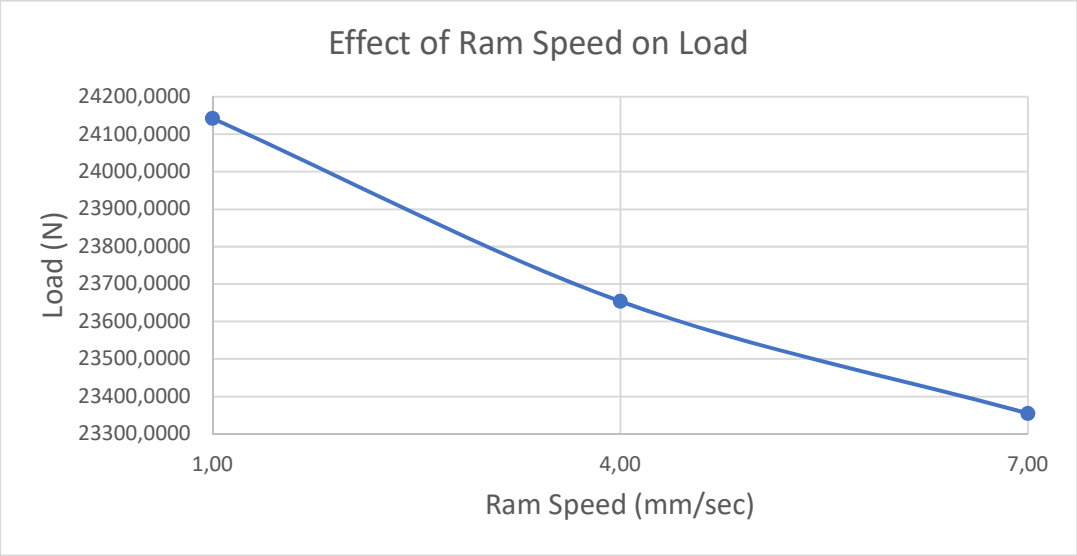

Figure 3.5: Effect of ram speed on load.

Analysis 19, 20 and 21 are taken into consideration for this comparison on figure 3.5 as an example.

3.1.2 Effective Strain

Effective Strain data are obtained from Deform 3-D software by having a section cut from middle of the workpiece. Following the division of a section, 70 different points are evenly spaced and distributed over the workpiece to ensure uniform analysis and interpretation of every location on the material. On the figure 3.6 given below, placed points and effective strain graph can be checked.

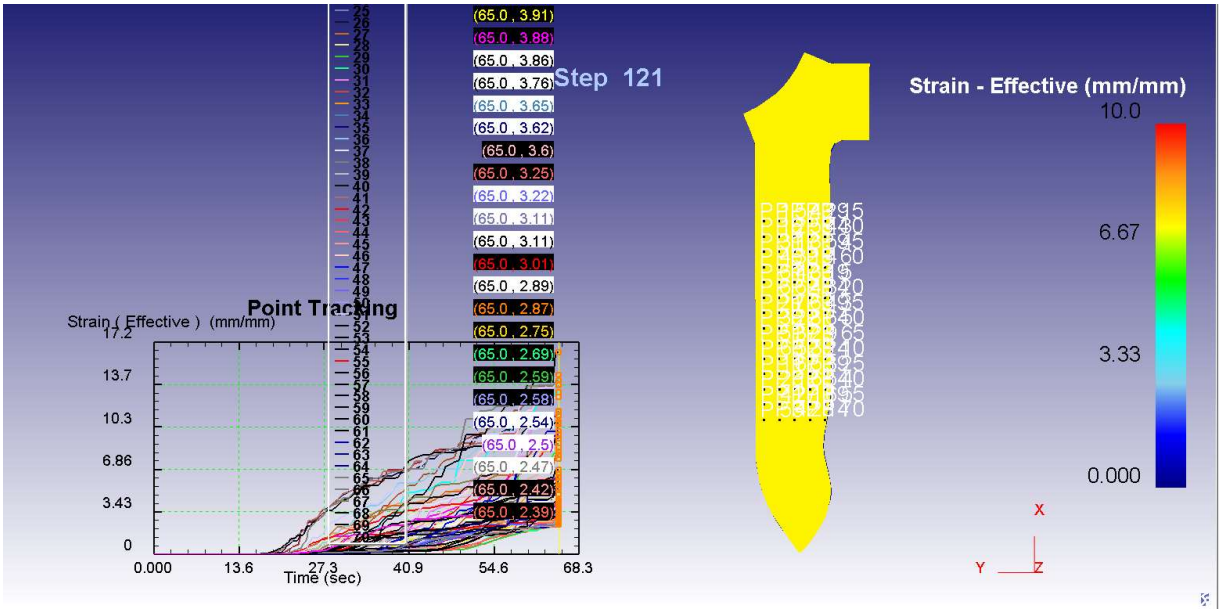

Figure 3.6: Effective strain graph of analysis 22 for every points.

After obtaining the strain graphs, all data is transferred from the graph to excel. Through the data in excel, average strain, standard deviation and strain inhomogeneity index are calculated. Strain inhomogeneity index, which can be seen in Eq.1, is the proportion of the standard deviation of strain to the average strain. Since average strain and standard deviation of the effective strain is already calculated through excel, strain inhomogeneity index is also calculated using Eq.3.1. Table 3.2 below displays the average and standard deviation of effective strain, as well as the strain inhomogeneity index.

$$Strain\ inhomogeneity\ index = \frac{\sigma_{str}}{\bar{X}_{str}} \tag{3.1}$$

Table 3.2: Strain outcomes for each analysis.

Analysis No	Average Strain	Standard Deviation	Strain Inhomogeneity Index
1	1,9429	0,37136	0,19114
2	2,0515	0,43580	0,21243
3	2,0129	0,38129	0,18942
4	1,6693	0,49696	0,29770
5	1,7071	0,546313	0,32002
6	1,8062	0,530194	0,29353
7	1,7990	0,682194	0,37919
8	1,7613	0,700576	0,39774
9	1,7248	0,703892	0,40808
10	2,4672	0,993612	0,40272
11	2,6301	0,981743	0,37325
12	2,4723	0,924078	0,37377
13	2,1826	1,040594	0,47675
14	2,1145	1,031274	0,48770
15	2,0507	1,020913	0,49781
16	2,1074	1,136270	0,5391
17	2,6562	1,134040	0,42693
18	2,1041	1,155692	0,54923
19	7	3,267226	0,48509
20	7,3690	3,295231	0,44717
21	7,7007	4,199322	0,54531
22	6,7316	3,704039	0,55024
23	6,8936	3,864396	0,56057
24	6,4251	3,495020	0,54396
25	5,2430	2,969268	0,56632
26	4,7425	2,807971	0,59207
27	6,1122	3,025577	0,49500

However, the impact of angle α, fillets on the die, and ram speed could be observed in the provided figures below.

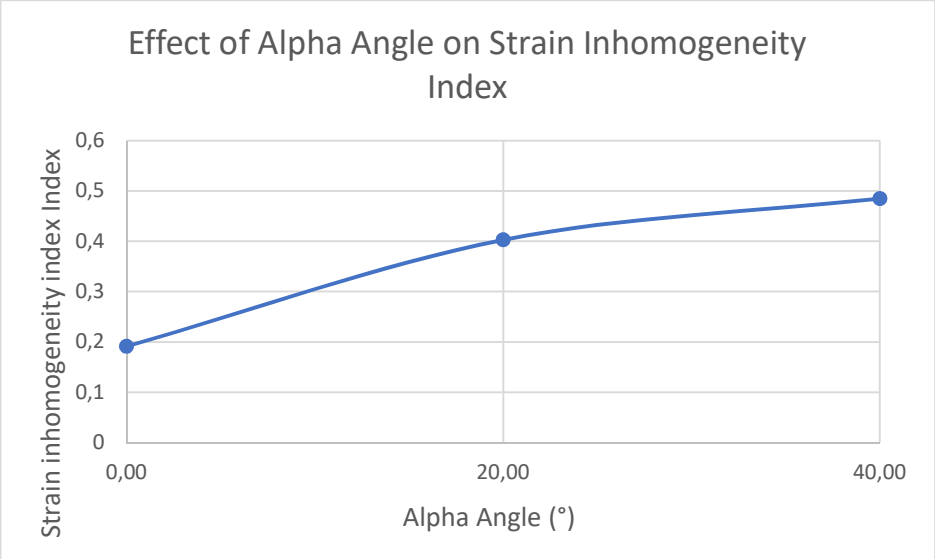

Figure 3.7: Effect of alpha angle on Strain inhomogeneity index.

On figure 3.7, analysis 7, 8 and 9 are taken as an example where other parameters are kept constant.

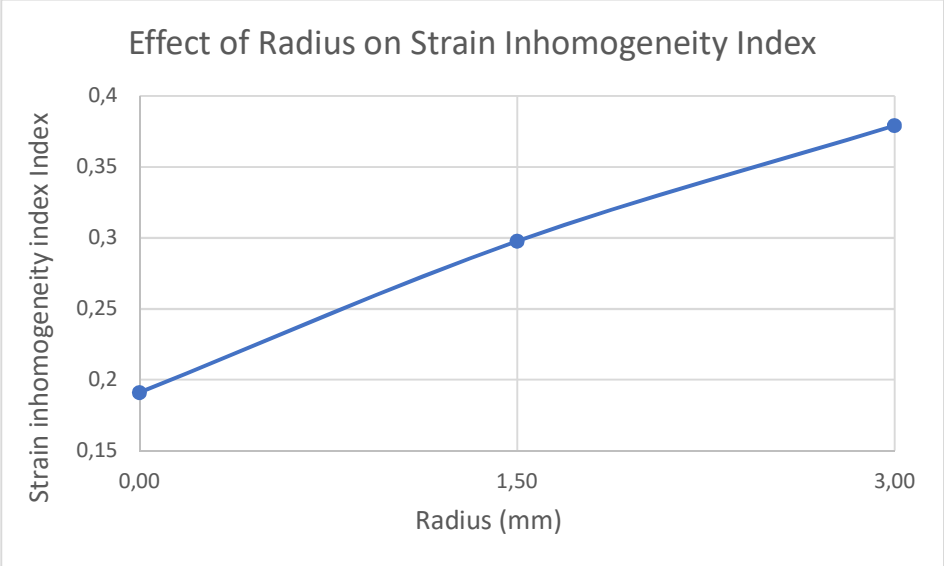

Figure 3.8: Effect of radius on strain inhomogeneity index.

Figure 3.8 illustrates the examination of examples 1, 4, and 7, while keeping other factors constant.

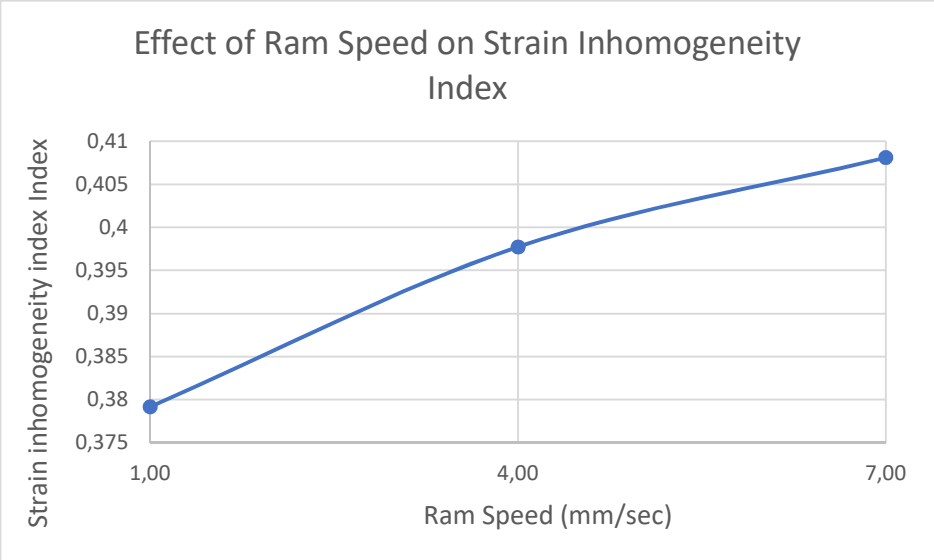

Figure 3.9: Effect of ram speed on Strain inhomogeneity index.

Figure 3.9 depicts the analysis of cases 1, 10, and 19, while keeping all other parameters constant.

As it is seen on the figures, results show that with the increase of angle α, there is a significant amount of increase in both average load and effective strain. As the planar twist angle rises, the length of contact between the material and plunger also increases. This increase results in elevated energy levels, thereby leading to a larger processing load. As a result, this inference matches with the reference study [29]. Increasing the ram speed in this research leads to the deduction with greater ram speed is associated with reduced processing load and decreased effective strain. This outcome could be explained by the fact that when the simulation is executed with a faster ram speed, the duration for the material to travel through its path decreases. Therefore, the material experiences less shear stress throughout the procedure. On the other hand, when the other parameter of radius is observed, it is seen that with the increase in the amount of radius, the material experiences less processing load and effective strain. This consequence is predicted because as the radius increases, the contact area between the material and die likewise increases. This leads to a decrease in shear stress, resulting in decreased processing load and effective strain.

3.2 DIE DESIGN AND SAFETY CONSIDERATIONS

The design parameters were determined using an equation that assigned equal importance to both the maximum load and the strain inhomogeneity index. To account for the differing ranges of maximum load and strain inhomogeneity index, the values were first normalized within the range of 0.1-0.9. The equation shown below utilised these normalized values.

Table 3.3: Normalized values of load and strain inhomogeneity data..

Analysis No	Normalize Max load(N)	Normalize Strain Inhomogeneity Index
1	0,29	0,10
2	0,56	0,15
3	0,34	0,10
4	0,12	0,32
5	0,25	0,36
6	0,29	0,31
7	0,20	0,48
8	0,25	0,51
9	0,10	0,53
10	0,62	0,52
11	0,59	0,47
12	0,51	0,47
13	0,30	0,67
14	0,30	0,69
15	0,22	0,71
16	0,33	0,79
17	0,78	0,57
18	0,40	0,81
19	0,90	0,69
20	0,79	0,61
21	0,81	0,81
22	0,78	0,82
23	0,70	0,84
24	0,76	0,80
25	0,54	0,85
26	0,51	0,90
27	0,67	0,71

The left side of this equation is named as 'objective function'. The right side of the equation is formed by using the values in the table numbered 3.3. In this table, objective function values are obtained for each analysis.

Table 3.4: Values of objective function.

Objective Function
0,20
0,35
0,22
0,22
0,31
0,30
0,34
0,38
0,32
0,57
0,53
0,49
0,49
0,49
0,47
0,56
0,67
0,61
0,79
0,70
0,81
0,80
0,77
0,78
0,70
0,70
0,69

$$Objective\ Function = (0.5 \times Max\ Load) + (0.5 \times Strain\ Inhomogeneity\ Index) \quad (3.2)$$

In this table, the parameters in the analysis with the lowest value which is 0.20 was taken as design parameters. As a result of FE analysis, all outcomes such as strain inhomogeneity and maximum load are discussed. According to these results and discussion, die option 1, which is the die used in analysis 1, is selected. During the selection process, the analysis which yields the lowest average of maximum load and of strain inhomogeneity is taken. The die selected and used in analysis 1 can be checked in the figure 3.10 below.As can be seen in Table 2.1, the design parameters of analysis number 1 are twisted channel angle 0, radius value 0, and ram speed 1.

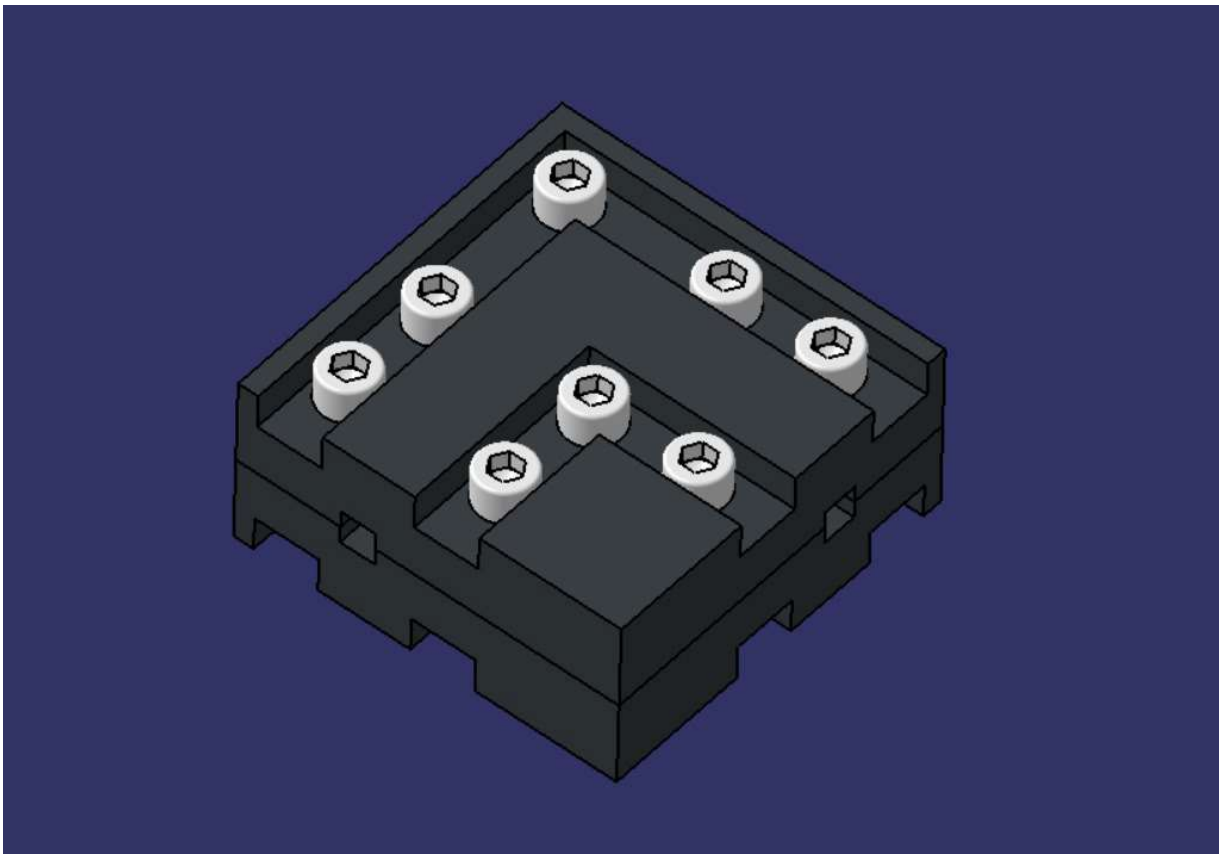

Figure 3.10: 3-D Model of the selected die.

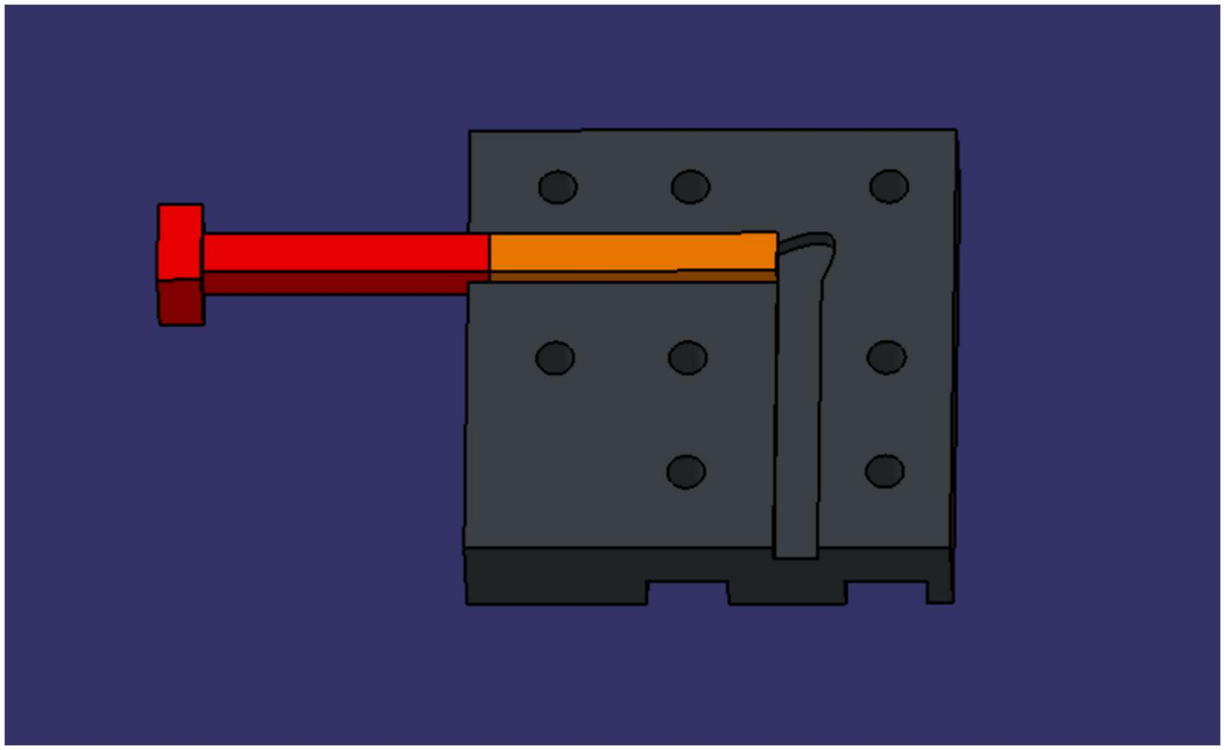

Figure 3.11: 3-D Model of the selected die.

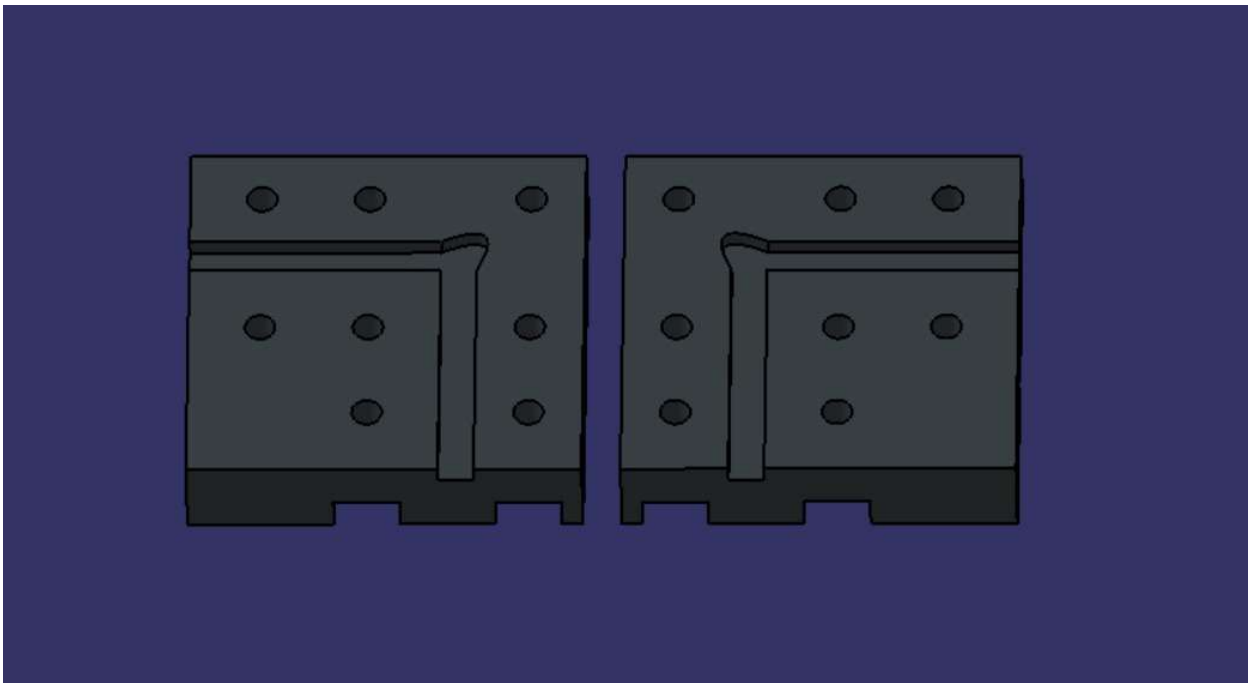

Figure 3.12: 3-D Model of the selected die.

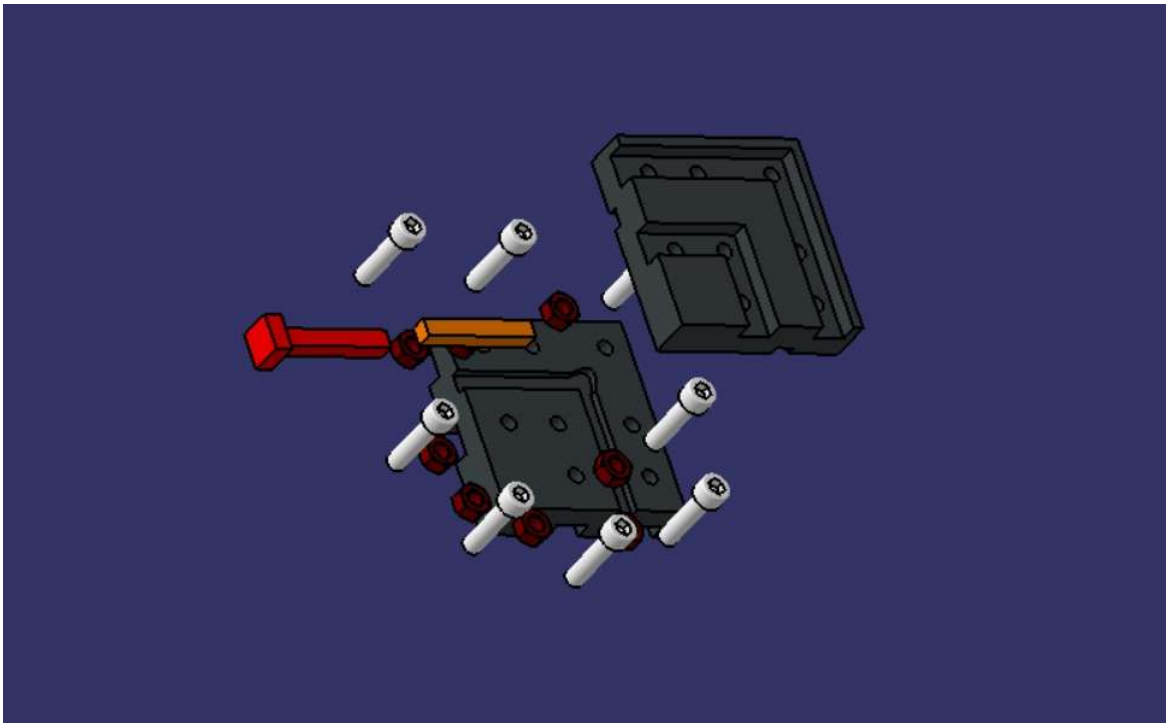

Figure 3.13: Exploded view of selected die.

3.2.1 Safety Control of Components and Material Selection

In this section, the safety calculations of all used components, including plunger, die and bolts are done and controlled in order to ensure that the process is completed without failure.

Table 3.1 indicates that the plunger sustains a peak load of 19951.7484 N during the process. In addition, the plunger material is selected to be H13 Tool Steel, a material with a yield strength of 1000 MPa. The safety factor of the plunger may be seen below, considering this load.

$$\sigma_p = \frac{F}{A} = \frac{19951.7484}{10 * 10} = 199.5175\ MPa \tag{3.6}$$

$$n_p = \frac{S_y}{\sigma_p} \tag{3.7}$$

$$n_p = \frac{1000}{199.5175} = 5.01 \tag{3.8}$$

The safety factor of plunger against the maximum load is found to be 5.01 and ensured that the plunger will not fail against the maximum load.

The die's safety control is also evaluated in relation to the peak load of 19951.7484 N. For the calculation, the die material used is H13 Tool Steel, which matches the material used for the plunger. The safety factor of the die may be seen below, taking into account this load.

$$\sigma_p = \frac{F}{A} = \frac{19951.7484}{(50*110)-10*10} = 3.6948\ MPa \tag{3.3}$$

$$n_d = \frac{S_y}{\sigma_d} \tag{3.4}$$

$$n_p = \frac{1000}{3.6948} = 270.68 \tag{3.5}$$

The die has a safety factor of 270.68 against the peak load, ensuring that it will not fail under the maximum load.

The safety control of plunger is also evaluated in relation to buckling. For the calculation, specific material for plunger was chosen as H13 steel which has modulus of elasticity 215 GPa. The cross-sectional area of the plunger is 10x10 in millimeters. By using the formula inertia is calculated as 833.333mm^4. K value is set as 2 for fixed ends. The length of the plunger is 60mm.

$$P_{CR} = \frac{\pi EI}{(KL)^2} = \frac{\pi * 215000(\frac{10 * 10^3}{12})}{(2 * 60)^2} = 39088.1\ N \tag{3.9}$$

$$\sigma_{CR} = \frac{P_{CR}}{A} = \frac{39088.1}{10 * 10} 390.881\ MPa \tag{3.10}$$

$$n_p = \frac{S_y}{\sigma_{CR}} = \frac{1000}{390.881} = 2.558 \quad (3.11)$$

By using safety factor formula, it is found to be 2.558 and ensured that the plunger will not fail against buckling.

Additional attention is given to the bolt selection and safety control of bolts. During the selection process, the lateral load is first determined by finite element (FE) analysis. Subsequently, the bolt selection is made based on the lateral load and an assumed factor of safety. The computations in question may be verified here.

A lateral load value of 1.3e05 N was found on the z-axis of the load graph that was created by the 'DEFORM 3D' software. This value was determined based on the geometric of the die.

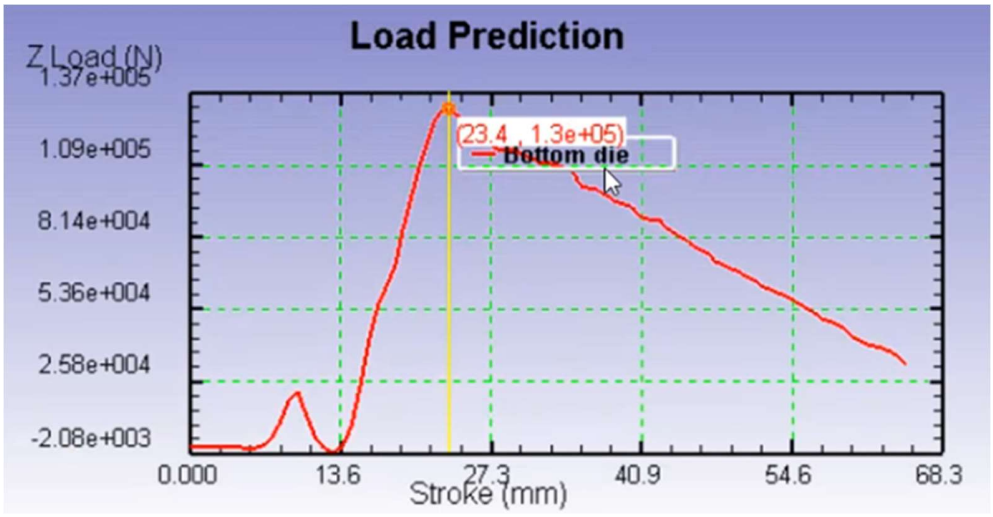

Figure 3.14: Lateral load graph of the die.

There were 8 bolts positioned on the die, and calculations were performed based on the number of bolts. The lateral force exerted on each bolt has been computed below.

$$F_b = \frac{130000N}{8} = 16250N \tag{3.12}$$

Throughout the calculations, the safety factor value of 5 was employed. In order to account for the potential occurrence of a lateral load exceeding the anticipated amount, a safety factor of 5 was used. Additionally, the grade of bolt is selected to be 12.9, which has a yield strength of 1100 MPa.

$$\sigma_b = \frac{F_b}{A} = \frac{16250}{\pi * r^2} \tag{3.13}$$

$$n_p = \frac{S_y}{\sigma_b} \tag{3.14}$$

$$5 = \frac{1100}{16250/(\pi * r^2)} \tag{3.15}$$

$$\sqrt{r^2} = \sqrt{25.511} \tag{3.16}$$

$$r = 4.85mm \sim 5\ mm \tag{3.17}$$

The M10 bolt is chosen based on dimension calculations, since it closely matches the calculated value according to the standards. As a result, the equipment was supplied with M10 DIN912 grade 12.9 hex socket screw bolts.

3.3. COST ANALYSIS

An important aspect of a design is the cost analysis.

Table 3.5: Cost Analysis

	Manufacturing Cost	Number of Amount	Cost
M10 DIN912 grade 12.9 Bolts	4,80₺	8	38,4₺
M10 Nuts	1,12₺	8	8,96₺
Die and Plunger	20.000₺	1	20.000₺
Workpiece	350₺	1	350₺
		TOTAL	**20.397,36₺**

The materials used in the cost analysis section of this thesis are given in the table 3.5. The cost of the screws and bolts used in the project was calculated by the suppliers by selecting the most suitable and robust ones among them. Die and plunger parts within the scope of the project were calculated with a detailed cost analysis in consultation with the supplier. For the workpiece part, the kilogram price of the steel type used was learned from the suppliers and the price calculation was made for the required part sizes. The cost analysis of these materials plays an important role in the financial planning and resource management of the project. The cost data obtained will contribute to the effective management of the project budget and the determination of cost reduction strategies when necessary.

3.4. COMPARISON

The results obtained in this study were compared with the results in the reference study [32]. The results obtained in this study show that the sum of strain inhomogeneity index and maximum load is minimum where the channel radius and twisted channel angle are 0 and 0 respectively. As a result of this process, the maximum load value was obtained as 19951.7484N. This value, selected as maximum load, is the average of a certain stroke range. During the analysis, sudden very high increases and decreases in load were observed inconsistently. Therefore, the average load value in certain stroke intervals is considered as the maximum load value. In the reference study, the maximum load value obtained with the same twisted channel angle values is 13500N. In addition, the average effective strain values obtained were compared. As a result of the die and ram speed used in this study, the effective strain was obtained as 1.9429. On the other hand, in the reference study, the effective strain value was determined as 0.8. It is thought that the main reason for these differences is that the workpiece does not completely fill the twisted angled section in the channel, as stated in the reference study.

3.5. ARTIFICAL NEURAL NETWORK (ANN)

ANN is performed based on 27 analyses. In this section, the performance of ANN, prediction of average load, strain and strain inhomogeneity index are presented for every parameter set. On the figure 3.15 below, the training and testing performance of the average load is given.

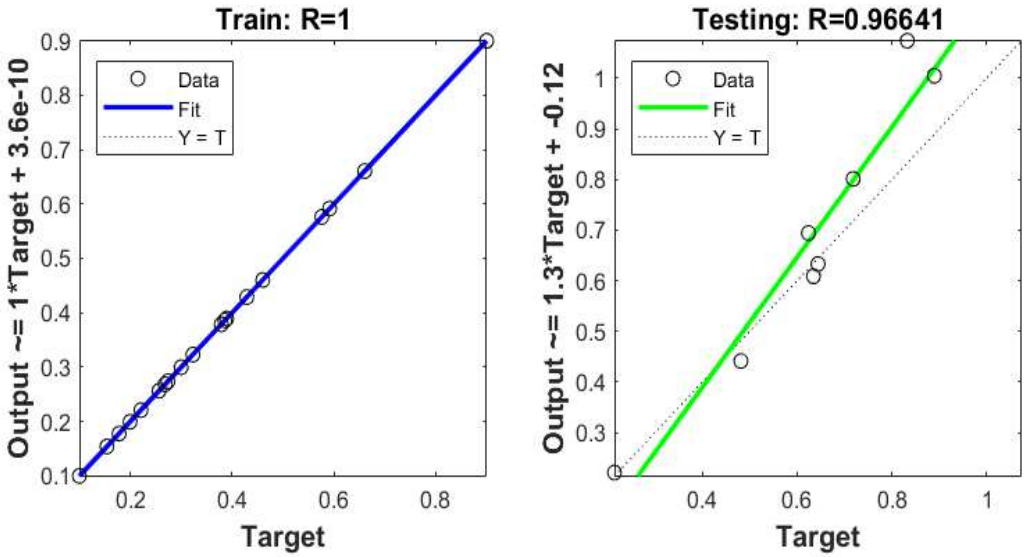

Figure 3.15: Training and testing regression values on average load.

Figure 3.16 shows the performance of prediction on average strain below.

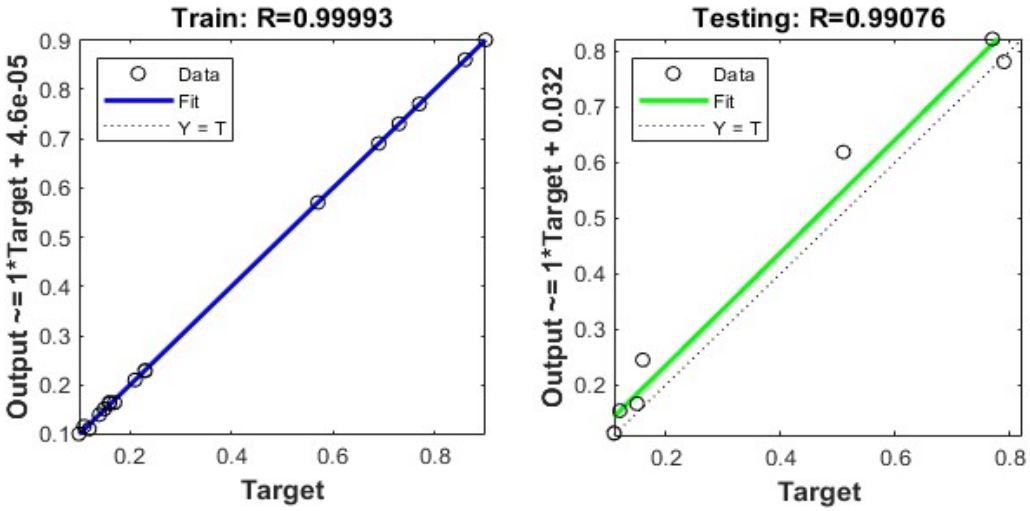

Figure 3.16: Training and testing regression values on average strain.

Figure 3.17 below shows the performance of the prediction on strain inhomogeneity index.

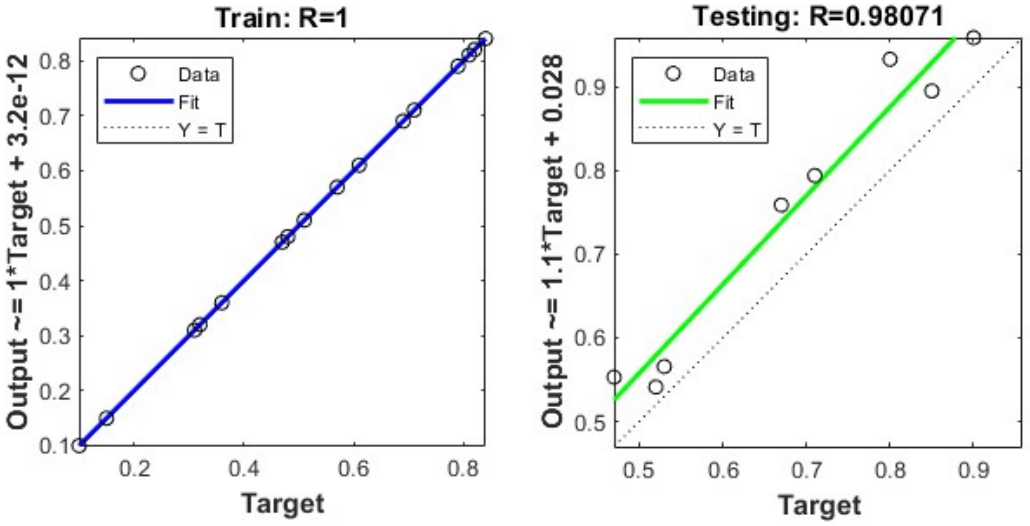

Figure 3.17: Training and testing regression values on strain inhomogeneity index.

At the beginning of training an Artificial Neural Network (ANN), there are unexpectedly low regression values below 0.8 seen in both the training and testing stages. Consequently, the percentage of average error and maximum error for average load, strain inhomogeneity index, and effective strain values surpassed the initial predictions, reaching 120% and 150% respectively. As previously mentioned, this is due to the high fluctuations in values in FE analyses. When using a second-order smoothing technique to extract data from the graphs and reattempting the employment of an ANN, a substantial reduction is noted in the regression values for both training and testing. Consequently, this also led to a reduction in the average and maximum percentage error to appropriate levels. After this procedure is applied, for average effective strain, average load, and strain inhomogeneity index, the average error rate is found to be 14.28%, 10.23 %, and 9.12% respectively. After several trials are employed, the regression values of effective strain, strain inhomogeneity index, and average load are to be observed as 0.99, 0.98, 0.96 respectively. As a result of these simulations, it can be interpreted that simulations with larger regression values provide more logical findings, leading to a drop in error rates.

4. CONCLUSION

In this study, average load and effective strain values are obtained at the end of analyses made with PTCAE process. 3-D FE simulations are performed to investigate how different parameters affect the average load and effective strain values on the material. Totally, 27 different analyses were applied to the material, by changing the ram speed, inserting a radius on dies, and changing the planar twist angle (α). During the analysis of load graphs, it was seen that there were unexpected oscillations while defining the maximum load. To minimize these fluctuations, a second-order smoothing approach is used, which greatly simplified the testing process. Subsequently, all the impacts of parameters in the simulations are compared with one another, separately. Upon comparing all of the factors' effects on the load and strain data, it is noticeable that the planar twist angle has the greatest influence on the load and strain values. In contrast, the speed at which the ram moves have the minimal impact on the behavior of the material. In general, the PTCAE method has the ability to apply more shear strain due to the presence of the additional shear angle, denoted as α.

Following the completion of finite element analyses, the MATLAB software is employed to apply artificial neural networks (ANN) and construct a model that accurately represents the correlation between the input parameters of the PTCAE process (plunger speed, die radius, and angle α and the corresponding values of average load, effective strain, and strain inhomogeneity index. The values are derived from FE studies. Subsequently, ANN was trained using a dataset including input characteristics and their associated target values. The objective is to forecast target values based on the provided inputs, with the aim of minimizing the error rate and maximizing the regression values. The input matrix is built in three generated network files, including the parameters of radius, angle α, and plunger speed. Afterwards, three target matrices are generated utilizing the data obtained from FE analyses. These matrices describe the variation of strain, strain inhomogeneity index, and the average load individually. Initially, the trial-and-error approach is used to determine the optimal number of hidden neurons that would provide improved regression results. After conducting several trials, it has been determined that the most favorable results are attained by using 7 hidden neurons for average load, and strain inhomogeneity index. However, using 2 hidden neurons for effective strain simulations produced the optimal outcome. Following that, the network is initialized using the "newfit" command, which generates the network by using input and target matrices, as well as the specified number of hidden neurons. The data are subsequently separated into a train set and a test set so that the ANN can undergo training. In conclusion of the ANN training, testing and target errors are exported to excel. As stated before, the first training phase is characterized by the occurrence of unexpected and increased error rates. However, because of the influence of several factors such as the number of hidden neurons and the division rate of the training and test sets, error rates might vary significantly from the predicted values. At the end of couple of trials, the optimal number of hidden neurons is found, and error rates showed a significant decrease up to approximately 10%, which is an acceptable rate for all trained average load, average strain and strain inhomogeneity index.

5. APPENDICES

```
% Create Network
numHiddenNeurons = 2;  % Adjust as desired
net = newfit(inputs,targets,numHiddenNeurons);
net.trainParam.goal=1e-6
net.divideParam.trainRatio = 70/100;  % Adjust as desired
net.divideParam.valRatio = 0/100;  % Adjust as desired
net.divideParam.testRatio = 30/100;  % Adjust as desired

% For help on training function 'trainlm' type: help trainlm
% For a list of all training functions type: help nntrain
net.trainFcn = 'trainlm';  % Levenberg-Marquardt
% Choose a Performance Function
% For a list of all performance functions type: help nnperformance
net.performFcn = 'mae'; % Mean absolute error

% Train and Apply Network
[net,tr] = train(net,inputs,targets);
outputs = sim(net,inputs);
error=outputs-targets;
trOut = outputs(tr.trainInd);
% vOut = outputs(tr.valInd)
tsOut = outputs(tr.testInd);
trTarg = targets(tr.trainInd);
% vTarg = targets(tr.valInd)
tsTarg = targets(tr.testInd);
trerror=trOut-trTarg;
% verror=vOut-vTarg;
tserror=tsOut-tsTarg;
```

Figure 5.1: Matlab codes applied for creating, training and applying network.

```
xlswrite('Hata',error)
xlswrite('Hata',targets,'A2:AC2')
xlswrite('Hata',trerror, 'A10:S10')
xlswrite('Hata',trTarg,'A11:S11')
% xlswrite('Hata',verror, 'A17:E17')
% xlswrite('Hata',vTarg,'A18:E18')
xlswrite('Hata',tserror, 'A25:H25')
xlswrite('Hata',tsTarg,'A26:H26')
% Plot
plotperf(tr)
plotfit(net,inputs,targets)
plotregression(targets,outputs)
```

Figure 5.2: Matlab codes for exporting data to excel.

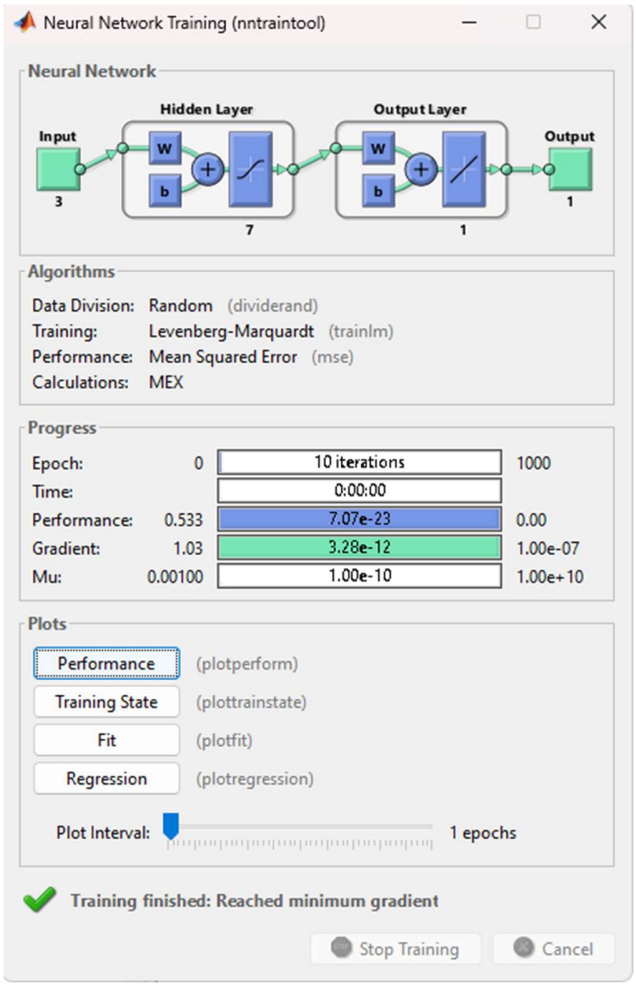

Figure 5.3: Training display of ANN.

6. REFERENCES

[1] R. Z. Valiev, R. K. Islamgaliev, and I. V Alexandrov, “Bulk nanostructured materials from severe plastic deformation.”

[2] S. Ogut, H. Kaya, A. Kentli, K. Ozbeyaz, M. Sahbaz, and M. Ucar, “Investigation of strain inhomogeneity in hexa-ECAP processed AA7075,” *Archives of Metallurgy and Materials*, vol. 66, no. 2, pp. 431–436, 2021, doi: 10.24425/amm.2021.135875.

[3] L. Bhatta, A. Pesin, A. P. Zhilyaev, P. Tandon, C. Kong, and H. Yu, “Recent development of superplasticity in aluminum alloys: A review,” *Metals*, vol. 10, no. 1. MDPI AG, Jan. 01, 2020. doi: 10.3390/met10010077.

[4] H. Kumar, K. Devade, D. Pratap Singh, J. M. Giri, M. Kumar, and V. Arun, “Severe plastic deformation: A state of art,” *Mater Today Proc*, 2023, doi: 10.1016/j.matpr.2023.02.194.

[5] R. Z. Valiev, R. K. Islamgaliev, and I. V Alexandrov, “Bulk nanostructured materials from severe plastic deformation.”

[6] K. Özbeyaz *et al.*, “International Marmara Sciences Congress (Imascon 2020-Autumn) Proceedings Book.”

[7] K. Edalati and Z. Horita, “A review on high-pressure torsion (HPT) from 1935 to 1988,” *Materials Science and Engineering: A*, vol. 652. Elsevier Ltd, pp. 325–352, Jan. 15, 2016. doi: 10.1016/j.msea.2015.11.074.

[8] Y. Beygelzimer, V. Varyukhin, S. Synkov, and D. Orlov, “Useful properties of twist extrusion,” *Materials Science and Engineering: A*, vol. 503, no. 1–2, pp. 14–17, Mar. 2009, doi: 10.1016/j.msea.2007.12.055.

[9] J. M. Torralba, C. E. Da Costa, and F. Velasco, “P/M aluminum matrix composites: an overview.”

[10] J. Huang, Y. T. Zhu, D. J. Alexander, X. Liao, T. C. Lowe, and R. J. Asaro, “Development of repetitive corrugation and straightening,” *Materials Science and Engineering: A*, vol. 371, no. 1–2, pp. 35–39, Apr. 2004, doi: 10.1016/S0921-5093(03)00114-X.

[11] Z. Zhang, L. Yuan, M. Zheng, Q. Wei, D. Shan, and B. Guo, “Achievement of high strength and good ductility in the large-size AZ80 Mg alloy using a designed multi-directional forging process and aging treatment,” *J Mater Process Technol*, vol. 311, Jan. 2023, doi: 10.1016/j.jmatprotec.2022.117828.

[12] J. Wu, M. Ebrahimi, S. Attarilar, C. Gode, and M. Zadshakoyan, “Cyclic Extrusion Compression Process for Achieving Ultrafine-Grained 5052 Aluminum Alloy with

Eminent Strength and Wear Resistance," *Metals (Basel)*, vol. 12, no. 10, Oct. 2022, doi: 10.3390/met12101627.

[13] M. B. Karamiş, V. Erturun, and F. N. Sari, "Investigation on effects of reciprocating extrusion process on microstructure of AA 6061 based composites," *Materials Science and Technology (United Kingdom)*, vol. 28, no. 12, pp. 1379–1384, Dec. 2012, doi: 10.1179/1743284712Y.0000000086.

[14] D. H. Shin, J.-J. Park, Y.-S. Kim, and K.-T. Park, "Constrained groove pressing and its application to grain refinement of aluminum," 2002. [Online]. Available: www.elsevier.com/locate/msea

[15] Z. Xin, W. Jin-feng, and J. Tian-fuz, "ScienceDirect Gray Cast Iron With Directional Graphite Flakes Produced by Cylinder Covered Compression Process." [Online]. Available: www.sciencedirect.com

[16] E. Tolouei, M. R. Toroghinejad, V. Yousefi Mehr, and H. Monajati, "A combination of aluminium strip and brass mesh to process a refined structure composite via accumulative roll bonding: A characterization study," *Mater Charact*, vol. 205, Nov. 2023, doi: 10.1016/j.matchar.2023.113360.

[17] M. V. Naik, N. Narasaiah, P. Chakravarthy, and R. A. Kumar, "Microstructure and mechanical properties of friction stir processed Zn-Mg biodegradable alloys," *J Alloys Compd*, vol. 970, Jan. 2024, doi: 10.1016/j.jallcom.2023.172160.

[18] D. C. Hofmann and K. S. Vecchio, "Submerged friction stir processing (SFSP): An improved method for creating ultra-fine-grained bulk materials," *Materials Science and Engineering: A*, vol. 402, no. 1–2, pp. 234–241, Aug. 2005, doi: 10.1016/j.msea.2005.04.032.

[19] R. Z. Valiev and T. G. Langdon, "Principles of equal-channel angular pressing as a processing tool for grain refinement," *Progress in Materials Science*, vol. 51, no. 7. pp. 881–981, Sep. 2006. doi: 10.1016/j.pmatsci.2006.02.003.

[20] Z. Horita, T. Fujinami, M. Nemoto, and T. G. Langdon, "Improvement of mechanical properties for Al alloys using equal-channel angular pressing."

[21] A. I. Alateyah *et al.*, "Improved corrosion behavior of AZ31 alloy through ECAP processing," *Metals (Basel)*, vol. 11, no. 2, pp. 1–19, Feb. 2021, doi: 10.3390/met11020363.

[22] M. Furukawa, Z. Horita, M. Nemoto, and T. G. Langdon, "Review Processing of metals by equal-channel angular pressing."

[23] R. Z. Valiev and T. G. Langdon, "5 Developments in the use of ECAP processing for grain refinement DEVELOPMENTS IN THE USE OF ECAP PROCESSING FOR GRAIN REFINEMENT," 2006.

[24] M. J. Qarni, G. Sivaswamy, A. Rosochowski, and S. Boczkal, “Effect of incremental equal channel angular pressing (I-ECAP) on the microstructural characteristics and mechanical behaviour of commercially pure titanium,” *Mater Des*, vol. 122, pp. 385–402, May 2017, doi: 10.1016/j.matdes.2017.03.015.

[25] S. M. Alavizadeh, K. Abrinia, and A. Parvizi, “Twisted Multi Channel Angular Pressing (TMCAP) as a Novel Severe Plastic Deformation Method,” *Metals and Materials International*, vol. 26, no. 2, pp. 260–271, Feb. 2020, doi: 10.1007/s12540-019-00319-x.

[26] M. Şahbaz, H. Kaya, and A. Kentli, “A new severe plastic deformation method: thin-walled open channel angular pressing (TWO-CAP),” *International Journal of Advanced Manufacturing Technology*, vol. 106, no. 3–4, pp. 1487–1496, Feb. 2020, doi: 10.1007/s00170-019-04748-1.

[27] M. Rassa, G. Azadkoli, M. Eftekhari, A. Fata, and G. Faraji, “Effects of Equal Channel Angular Pressing (ECAP) Process with an Additional Expansion-Extrusion Stage on Microstructure and Mechanical Properties of Mg-9Al-1Zn,” 2021. [Online]. Available: http://jmatpro.iaun.ac.ir

[28] M. Shamsborhan and A. Shokuhfar, “A planar twist channel angular extrusion (PTCAE) as a novel severe plastic deformation method based on equal channel angular extrusion (ECAE) method,” *Proc Inst Mech Eng C J Mech Eng Sci*, vol. 228, no. 12, pp. 2246–2250, 2014, doi: 10.1177/0954406213515645.

[29] A. Shokuhfar and M. Shamsborhan, “Finite element analysis of planar twist channel angular extrusion (PTCAE) as a novel severe plastic deformation method,” *Journal of Mechanical Science and Technology*, vol. 28, no. 5, pp. 1753–1757, 2014, doi: 10.1007/s12206-014-0321-1.

[30] M. Shamsborhan and A. Shokuhfar, “A planar twist channel angular extrusion (PTCAE) as a novel severe plastic deformation method based on equal channel angular extrusion (ECAE) method,” *Proc Inst Mech Eng C J Mech Eng Sci*, vol. 228, no. 12, pp. 2246–2250, 2014, doi: 10.1177/0954406213515645.

[31] N. Pardis and R. Ebrahimi, “Deformation behavior in Simple Shear Extrusion (SSE) as a new severe plastic deformation technique,” *Materials Science and Engineering: A*, vol. 527, no. 1–2, pp. 355–360, Dec. 2009, doi: 10.1016/j.msea.2009.08.051.

[32] M. Shamsborhan and M. Ebrahimi, “Production of nanostructure copper by planar twist channel angular extrusion process,” *J Alloys Compd*, vol. 682, pp. 552–556, Oct. 2016, doi: 10.1016/j.jallcom.2016.05.012.